

**Interface of Gallium-Based Liquid Metals: Oxide Skin,
Wetting, and Applications**

Journal:	<i>Nanoscale Horizons</i>
Manuscript ID	NH-FOC-02-2024-000067.R1
Article Type:	Review Article
Date Submitted by the Author:	10-Apr-2024
Complete List of Authors:	Kim, Ji-Hye; Seoul National University of Science & Technology, Department of Chemical Engineering Kim, Sooyoung; North Carolina State University, Chemical & Biomolecular Engineering Dickey, Michael; North Carolina State University, Chemical & Biomolecular Engineering So, Ju-Hee; Korea Institute of Industry and Technology Information/ KINITI Koo, Hyung-Jun; Seoul National University of Science & Technology

REVIEW

Interface of Gallium-Based Liquid Metals: Oxide Skin, Wetting, and Applications

Ji-Hye Kim^a, Sooyoung Kim^b, Michael D. Dickey^b, Ju-Hee So^{*c}, Hyung-Jun Koo^{*d}

Received 00th January 20xx,
Accepted 00th January 20xx

DOI: 10.1039/x0xx00000x

Gallium-based liquid metals (GaLMs) are promising for a variety of applications—especially as a component material for soft devices—due to the fluidic nature, low toxicity and reactivity, and high electrical and thermal conductivity comparable to solid counterparts. Understanding the interfacial properties and behaviors of GaLMs in different environments is crucial for most applications. When exposed to air or water, GaLMs form a gallium oxide layer with nanoscale thickness. This “oxide nano-skin” passivates the metal surface and allows for the formation of stable microstructures and films despite the high-surface tension of liquid metal. The oxide skin easily adheres to most smooth surfaces. While it enables effective printing and patterning of the GaLMs, it can also make the metals challenging to handle. The oxide also affects the interfacial electrical resistance of the metals. Its formation, thickness, and composition can be chemically or electrochemically controlled, altering the physical, chemical, and electrical properties of the metal interface. Without the oxide, GaLMs wet metallic surfaces but do not wet non-metallic substrates like polymers. The topography of the underlying surface further influences the wetting characteristics of the metals. This review outlines the interfacial attributes of GaLMs in air, water, and other environments and discusses relevant applications based on interfacial engineering. The effect of surface topography on wetting behaviors of the GaLMs is also discussed. Finally, we suggest important research topics for a better understanding of the GaLMs interface.

1 Introduction

Liquid metals that are liquid phase at or near room temperature have attracted attention as conductors for stretchable electronics, active materials for soft devices, and catalysts, among a number of emerging applications. However, most of the elemental liquid metals such as mercury, cesium, rubidium, and francium have problems in practical use due to their high toxicity, reactivity, and / or radioactivity. In contrast, gallium and gallium-based alloys have low toxicity. Plus, they have negligible vapor pressure.

Eutectic gallium indium (EGaln) and gallium indium tin alloys are the most commonly used gallium-based liquid metals (GaLMs). They are homogeneous liquids that have fluidic properties with low viscosity at room temperature. GaLMs have high electrical/thermal conductivity (Ga $\sim 3.9 \times 10^6$ S/m, 30.5 W/m·K, EGaln $\sim 3.4 \times 10^6$ S/m, 26.4 W/m·K, and Galinstan $\sim 3.3 \times 10^6$ S/m ~ 25.4 W/m·K), only one order of magnitude lower than copper metal¹⁻³. A thin gallium oxide layer generally forms on the surface of GaLMs in air or aqueous environments. The surface oxide, which is a solid-phase film, encapsulates the liquid metal, enabling the formation of stable microdroplets, thin films, or other non-spherical shapes. The surface oxide easily adheres to and pins on many solid substrates due to the various interactions such as van der Waals attraction and hydrogen bonding. While such a solid, adhesive oxide allows effective printing or patterning of GaLMs⁴, it can also make GaLMs difficult to handle because it sticks to surfaces that touch it. Moreover, the presence of an oxide decreases the interfacial conductivity relative to pure metal, and therefore its formation largely determines the interfacial resistance of GaLMs. Formation of such an oxide and its thickness and composition can be varied chemically, thermally, or electrochemically, which significantly affects the physical/chemical/electrical properties of the GaLMs interface.

^a Department of Energy and Chemical Engineering, Seoul National University of Science & Technology, 232 Gongneung-ro, Nowon-gu, Seoul, 01811, Republic of Korea

^b Department of Chemical and Biomolecular Engineering, North Carolina State University, Raleigh, NC, 27695, USA. Email: mddickey@ncsu.edu

^c Material & Component Convergence R&D Department, Korea Institute of Industrial Technology, Ansan-si, 15588, Republic of Korea. Email: jso@kitech.re.kr

^d Department of Chemical & Biomolecular Engineering, Seoul National University of Science & Technology, 232 Gongneung-ro, Nowon-gu, Seoul, 01811, Republic of Korea. Email: hjkoo@seoultech.ac.kr

The surface of GaLMs oxidizes in the presence of air or water. In air (oxygen), the metals form a native oxide layer on the surface. The oxide is an amorphous Ga_2O_3 . Dissolved metals in GaLMs with a more favorable Gibbs energy of reaction, such as Al, can change the composition of the oxide⁵. In water, an oxide also forms (either due to dissolved oxygen or by direct reaction with water). Over time, the oxide converts to GaOOH . The GaOOH can exfoliate from the system to form, crystalline rod-like shapes^{6, 7}. Water can also serve as an electrolyte to facilitate electrochemical reactions that drive oxidation or reduction of the surface⁸. In addition, water can contain acids or bases that can dissolve the oxide at low or high pH.

GaLMs can form metal-metal bonds with many metals and therefore show favorable wetting behavior on most metallic surfaces in the absence of the oxide. On the other hand, GaLMs without the oxide generally show poor wetting behavior on non-metallic surfaces such as polymers. The texture or topography on the substrate further enhances the wetting or non-wetting characteristics of GaLMs, which is governed by their wetting states: Wenzel state or Cassie-Baxter state. Thus, interfacial properties and behaviors of GaLMs greatly depends on their environment and a proper understanding of these is crucial.

This review focuses on the interfacial properties and characteristics of GaLMs when exposed to different environments of air, water, acid and base, metals, and other materials, as summarized in Figure 1. Recent reviews have focused on the interfacial tension and surface chemistry of liquid metal^{9, 10}, interfacial properties for patterning⁴, interface engineering for particle production and utilization¹¹, and surface modification for sensor and actuator applications¹². Naturally, while there is some overlap by necessity, the present review is distinguished by a focus on the connection between the interfacial properties and interactions with interfacing matter. We discuss how the interfacial properties of GaLMs are intentionally manipulated to exploit them in various applications. Research on the effect of surface topography on the wetting behaviors of the metals is also introduced. Lastly, we suggest several potentially important studies which needs to be done for better understanding of the metals' interface.

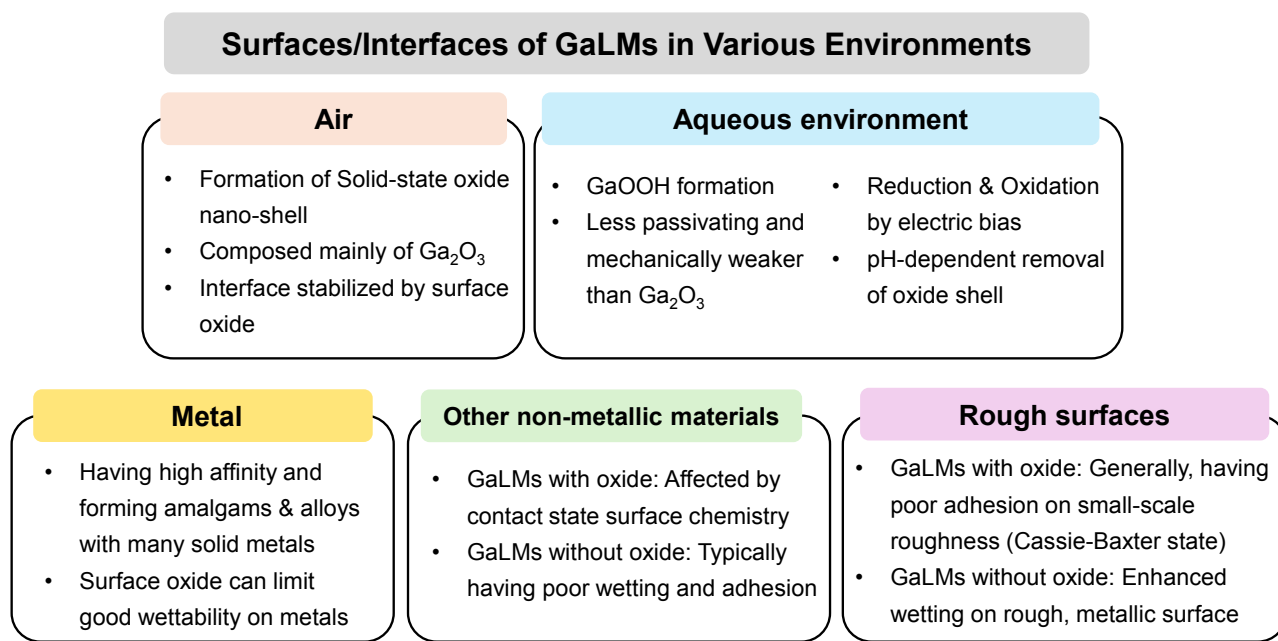
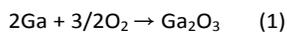


Fig. 1 Schematic of interfaces of GaLMs on various environments.

2 Interface with air

The surface of GaLMs oxidizes rapidly after even a brief exposure to oxygen as low as 10^{-7} Torr. At steady state, the oxide is ~ 2 -5 nm thick (several studies report it to be ~ 3 nm). Previous high resolution X-ray photoelectron spectroscopy (XPS) has shown that the oxide skin is composed mainly of Ga_2O_3 as shown in Fig. 2(a), although small amounts of Ga_2O and In_2O_3 may exist underneath the Ga_2O_3 ¹³⁻¹⁷. When the oxide is sputtered off in the absence of oxygen, other metals (such as In in the case of EGaIn) can preferentially go to the interface to lower the tension. However, when air is reintroduced, the surface reverts back to gallium oxide¹³. The preferential formation of gallium oxide can be explained by Gibbs free energy (ΔG_f) for the formation of oxides, which is most negative for gallium compared to indium and tin (-998.3 kJ/mol for Ga_2O_3 , -830.7 kJ/mol for In_2O_3 and -515.8 kJ/mol for SnO_2) (Fig. 2(b))^{5, 18}. Based on this principle, it is possible to form oxides of other compositions by dissolving metals with a more favorable ΔG_f than Ga (e.g. Al). Ga^{3+} is that most energetically favorable oxidized state of Ga while Ga^{2+} is the least stable. The formation of gallium oxide is shown in Equation 1:



The growth of the native oxide is typically explained by Cabrera-Mott (CM) oxidation mechanism, which is associated with the oxidation process of group III metals, such as aluminium and gallium¹⁹⁻²¹. In this framework, initially bare metal reacts with O₂ to form a thin oxide layer. CM explains how this layer continues to grow despite the low diffusivity of oxygen through the oxide at room temperature. It also explains how it eventually stops growing (or slows significantly). In the CM mechanism, the first step involves O₂ adsorption on the surface of the metal oxide. Electrons from the Ga can tunnel through the oxide to form O²⁻ ions on the outside of the oxide, leaving behind a Ga cation on the inside of the oxide. The resulting electric field can drive the ions (either Ga cations and / or oxygen anions) through the oxide. The ions react to produce additional metal oxide. When the oxide gets thicker, the electric field diminishes to the point that the ions can no longer be driven through the oxide and the oxide growth slows significantly or stops.

Thus, the oxide layer typically stops growing in ambient conditions and passivates the internal liquid metal core from oxygen. Fig. 2(c) shows the EGaIn core wrapped with nanometer-thick gallium oxide, which varies from 0.5 to 5 nm depending on the conditions²²⁻²⁴. At room temperature, oxygen cannot penetrate through the oxide at any appreciable rate. Yet, at elevated temperatures (> 500 °C), the diffusion rate can increase²⁵⁻²⁷; thus, one way to increase the oxide thickness is via thermal oxidation. Thermal oxidation causes stress that creates microfractures in the shell, allowing the In or Sn-enriched interlayer to flow out and oxidize, leading to the formation of additional oxide shell such as indium oxide and tin oxide^{27, 28}. Electrochemical oxidation can also make the oxide thicker (see section below).

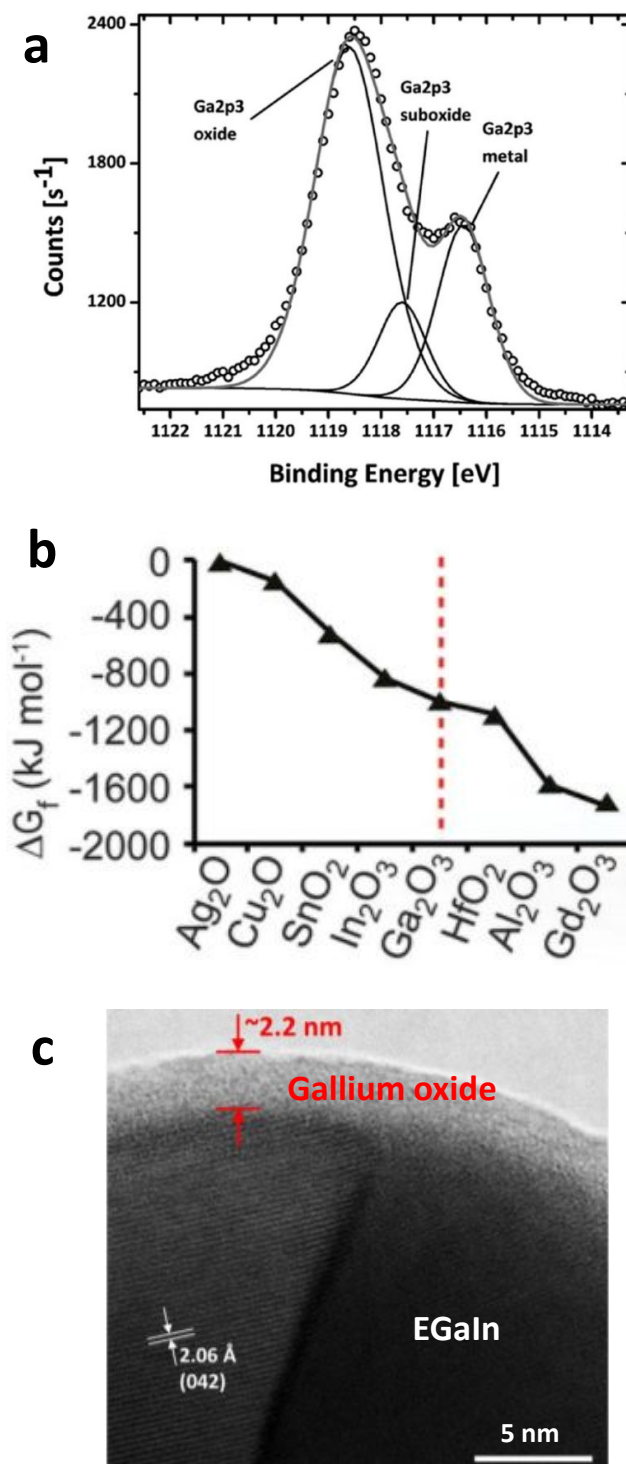


Fig. 2 Attributes of oxide skin of GaLMs. (a) High-resolution XPS spectrum of the Ga 2p region collected from the apex of EGaIn with the Ga₂O₃ native oxide. Reproduced with permission from ref. ¹⁷. Copyright 2012 American Chemical Society. (b) The Gibbs free energy (ΔG_f) of formation for metal oxides help predict favored composition of the surface oxide. Reproduced with permission from ref. ⁵. Copyright 2017 The American Association for the Advancement of Science. (c) HRSTEM bright field image for an EGaIn NP at the temperature of 173 K. An amorphous gallium oxide surface layer with a thickness of ~ 2.2 nm can be seen conforming to the surface of the metal. On the interior, phase-separated, solidified Ga and In at the low temperature are observed. Reproduced with permission from ref. ²⁴. Copyright 2019 Elsevier.

2.1 Injection of GaLMs in microfluidics

Injection of GaLMs into micro-channels is one of the simplest and most effective ways to mold GaLMs into a variety of shapes while encapsulating them into materials such as silicones with high structural stability. Pristine GaLMs without the surface oxide layer have high surface tension values (726.6 mN/m for Ga (at 30 °C)²⁹, 624 mN/m for EGaln (at 22 °C)³⁰, and 533 mN/m for Galinstan (at 25 °C)³¹). Normally, liquids with high surface tension try to bead up to minimize surface energy. However, GaLMs remain stable within microchannels due to the rapid formation of the oxide layer¹³. In Fig. 3(a), EGaln and mercury (Hg) were injected into the microchannel by applying pressure. Both liquid metals filled the channels if the applied pressure exceeds the Laplace pressure of the liquid, which opposes filling. After ceasing to apply pressure, EGaln stayed in the channel, but Hg instantaneously withdrew from the channel. The solid gallium oxide on the surface of EGaln stabilizes the metal in the channel. In the absence of the solid-oxide skin, Hg reflowed immediately upon ceasing to apply injecting pressure.

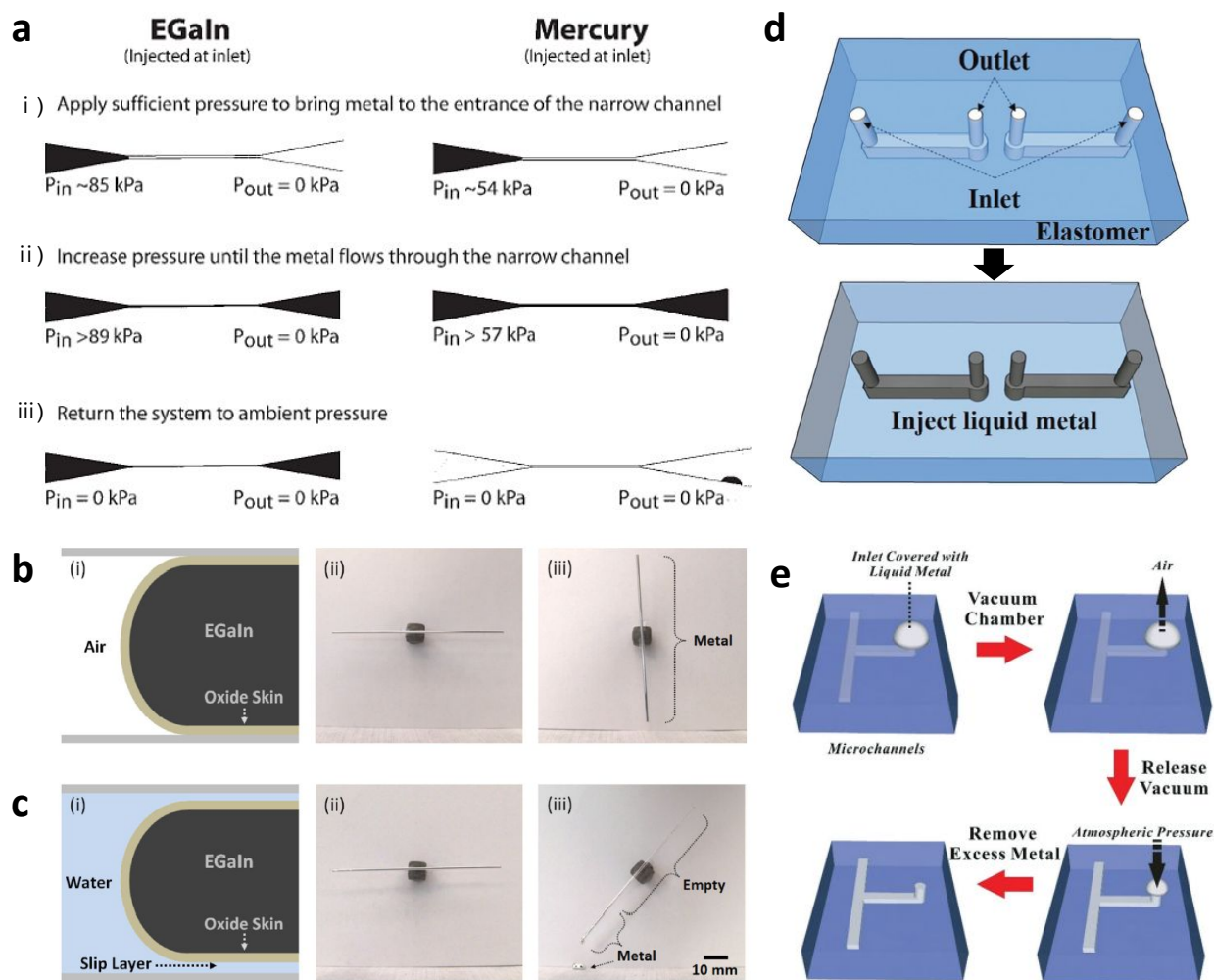


Fig. 3 Microfluidic filling principles using liquid metal. (a) Top-down optical photographs of EGaln (left) and Hg (right) in PDMS microchannels and their behavior under applied pressure. Reproduced with permission from ref. ³³. Copyright 2008 John Wiley and Sons. (b-c) The behavior of EGaln (b) in a dry capillary and (c) in a capillary prefilled with water: (b) (i, ii) The oxide layer directly contacts with the capillary wall. (iii) EGaln does not flow out after tilting the capillary vertically. (c) (i,ii) A water slip (or "lubrication") layer exists between the oxide layer and the capillary wall. (iii) EGaln flows out of the capillary due to gravity after tilting the capillary vertically. Reproduced with permission from ref. ⁷. Copyright 2014 American Chemical Society. (d) Schematic of fabrication process for filling microchannels with liquid metal by injection from an inlet toward an outlet. Reproduced with permission from ref. ³². Copyright 2015 Royal Society of Chemistry. (e) Schematic of vacuum process for filling microchannels with liquid metal using only an inlet and no outlet. Reproduced with permission from ref. ³³. Copyright 2017 Royal Society of Chemistry.

Moreover, the adhesive property of the oxide on GaLMs provides mechanical stability to the metal in microchannels. In a dry capillary, the oxide layer sticks to the inner wall of the capillary and keeps EGaln stable in the capillary without flowing out even under the influence of gravity (Fig. 3(b)). In a capillary prefilled with water, however, a water slip (or "lubrication") layer forms between the surface of EGaln and the inner wall of the capillary, which causes a plug of EGaln to easily flow out of the capillary

upon tilting (Fig. 3(c))⁷. Thus, the direct contact and adhesion at the interface between the oxide layer of GaLMs and the inner wall of microchannels is critical for the stability of GaLMs injected into channels.

Injection of GaLMs into a microchannel made by soft lithography or 3D printing is a common method to mold the metals due to its simplicity and convenience without complicated patterning techniques (Fig. 3(d)). This method has been widely used to fabricate liquid metal microchannels, antennas³⁴⁻³⁹, sensors⁴⁰⁻⁵¹, electronics^{49, 52-57}, conductors^{51, 58, 59}, and 3D structures⁶⁰⁻⁶². However, this method has some limitations, such as the need for extremely high pressure (~10 MPa) to fill a narrow channel (150 nm in width) or the possibility of trapping air, which can prevent the channel from being filled with the metal. The channel should also have an outlet to allow air to escape during liquid metal injection into the inlet. Vacuum filling, as shown in Fig. 3(e), addresses these issues^{33, 63}. Vacuum filling and injection both use pressure differentials to fill the metal. While injection requires an external pressure at the inlet to exceed that atmospheric pressure at the outlet, vacuum filling uses atmospheric pressure at the inlet and vacuum within the channels to achieve the pressure differential. First, liquid metal is placed at the inlet. Air in the channel is removed by placing the entire device in a vacuum chamber. Air can bubble through the liquid metal or diffuse through the silicone microchannel walls. Upon returning the chamber to atmospheric pressure, the negative pressure in the channel relative to the atmospheric pressure forces the liquid metal into the channel. Due to their negligible vapor pressure⁶⁴, GaLMs can be utilized in the vacuum filling process without concern for evaporation or boiling occurring at low pressure. The vacuum filling method is facile and hands-free, and it can cast deep and branching features without air trapping, leaks, or delamination. Moreover, it requires only one inlet and no outlets.

2.2 Direct writing of GaLMs

Direct writing is a technique based on an extrusion from a nozzle, which is a rapid, simple, scalable, customizable, and low-temperature process. Printing or patterning of GaLMs is enabled by direct writing on a substrate. This process requires stable adhesion of GaLMs to the substrate and movement of the nozzle to create mechanical stress (shear or tension) that can rupture the oxide (Fig. 4(a))⁶⁵. Thus, the choice of a proper substrate material is the key factor, as the printing process is primarily governed by the interaction between the substrate and the surface of GaLMs adhered to it^{66, 67}. The native gallium oxide skin on the surface of GaLMs tends to favor adhesion on hydrophilic surfaces⁶⁷. For example, the printing works better on oxygen plasma treated silicone than pristine silicone. The printed line width could be controlled by the inner diameter of the nozzle and printing velocity (Figs. 4(b) and (c))^{66, 68}. In a recent study, the minimum width of 1.9 μm was achieved using a nozzle diameter of 5 μm , as shown in Fig. 4(d)⁶⁸.

Furthermore, the gallium oxide skin enables the resulting pattern to maintain its printed shape against gravity and surface tension, allowing free-standing features without any encapsulating solid materials (Fig. 4(e)). It is possible to print EGaIn in the z-direction, which is a type of 3D printing technology. In this case, the liquid metal wire is elongated by the tensile force generated by adhesion between the oxide skin and the underlying substrate. With additional motion of the stage, 3D microstructures, such as self-supporting bridges, can be fabricated. Fig. 4(f) also shows the microstructures composed of sequentially stacked droplets of EGaIn, which is possible since the droplets form physical contact without coalescing into one bigger droplet⁶⁹.

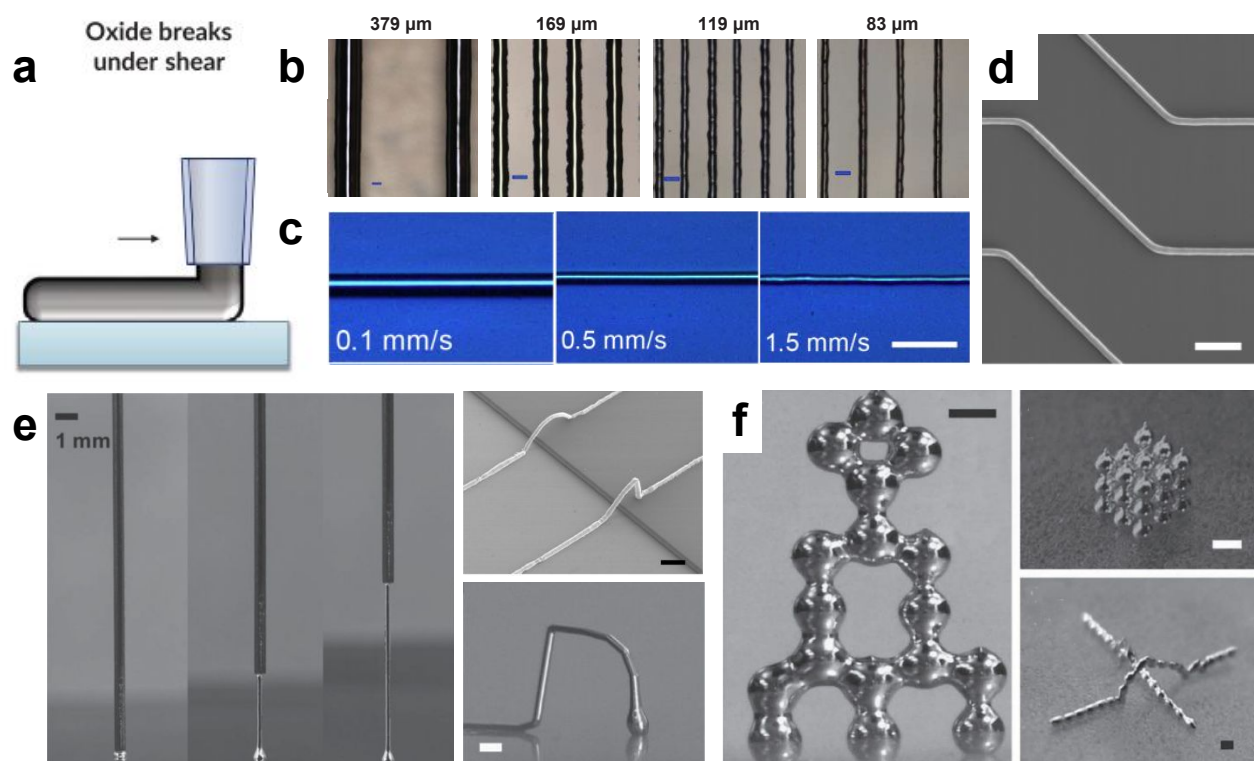


Fig. 4 Direct-writing and 3D printing of liquid metals by harnessing the stabilizing effects of the oxide skin. (a) Schematic of direct printing of GaLMs through shear force. Reproduced with permission from ref. ⁶⁵. Copyright 2020 John Wiley and Sons. (b) Optical microscope images of printed EGaIn lines on glass according to inner diameter of nozzles. Scale bar is 100 μm . Reproduced with permission from ref. ⁶⁶. Copyright 2014 John Wiley and Sons. (c) Optical microscope images of printed EGaIn lines on PET film according to printing velocities. Scale bar is 40 μm . (d) SEM image of 1.9 μm -width EGaIn lines. Scale bar is 10 μm . Reproduced with permission from ref. ⁶⁸. Copyright 2019 American Association for the Advancement of Science. (e) Sequential images of EGaIn wire vertically extruded from a nozzle and free-standing liquid metal arches. (f) Photographs of 3D microstructures composed of stacked droplets of EGaIn. Scale bar is 500 μm . Reproduced with permission from ref. ⁶⁹. Copyright 2013 John Wiley and Sons.

2.3 Soft electrode tip

The surface oxide layer of GaLMs has allowed the metals to form a soft electrode for non-destructive conformal electrical contacts. Such an electrode is useful especially for investigating the charge transport across organic thin films, such as self-assembled monolayers (SAMs). In molecular electronics, the studies of charge transport in organic molecules and at organic molecule-electrode interfaces have been crucial for understanding the relationship between molecular structures and electrical properties of molecular layers, e.g., injection tunnel current and current rectification^{70, 71}. Initially, the electrical properties of the single-molecular junction were typically studied by scanning tunneling microscopy (STM) and atomic force microscopy (AFM). However, the methods have technical difficulties and complexity of data interpretation. Also, it is challenging to achieve non-destructive, reproducible contacts between the top electrode and organic thin film⁷². To solve the problems, soft liquid metal electrodes consisting of a Hg droplet were utilized⁷³⁻⁷⁶. However, the use of mercury has been avoided due to its toxicity. GaLMs have been studied as an alternative material for the top electrode with low level of both toxicity and hazard⁷⁷⁻⁸¹. The oxide layer of GaLMs enables the metal to form a cone-shaped tip with micrometer-scale dimensions under ambient conditions, which makes semi-conformal and non-damaging contacts with SAM at a small area (Figs. 5(a) and (b))^{72, 82}. The cones form by adhering a droplet to a surface and then pulling on it as shown in Fig 5(a)⁷². Electrodes composed of GaLMs showed higher yields of junctions (80 ~ 100%) than the Hg electrode (< 20%)⁸³. The higher junction stability of the GaLM electrode results from the oxide layer, which prevents the liquid metal from penetrating the underlying material without affecting the current measurement⁸⁴. The EGaIn electrode can measure the tunneling current through the SAM of a short-chain alkyl group ($n = 1 \sim 6$) (Fig. 5(c))^{72, 85}. A recent review has summarized the use of such soft electrodes for characterizing SAMs⁸⁶.

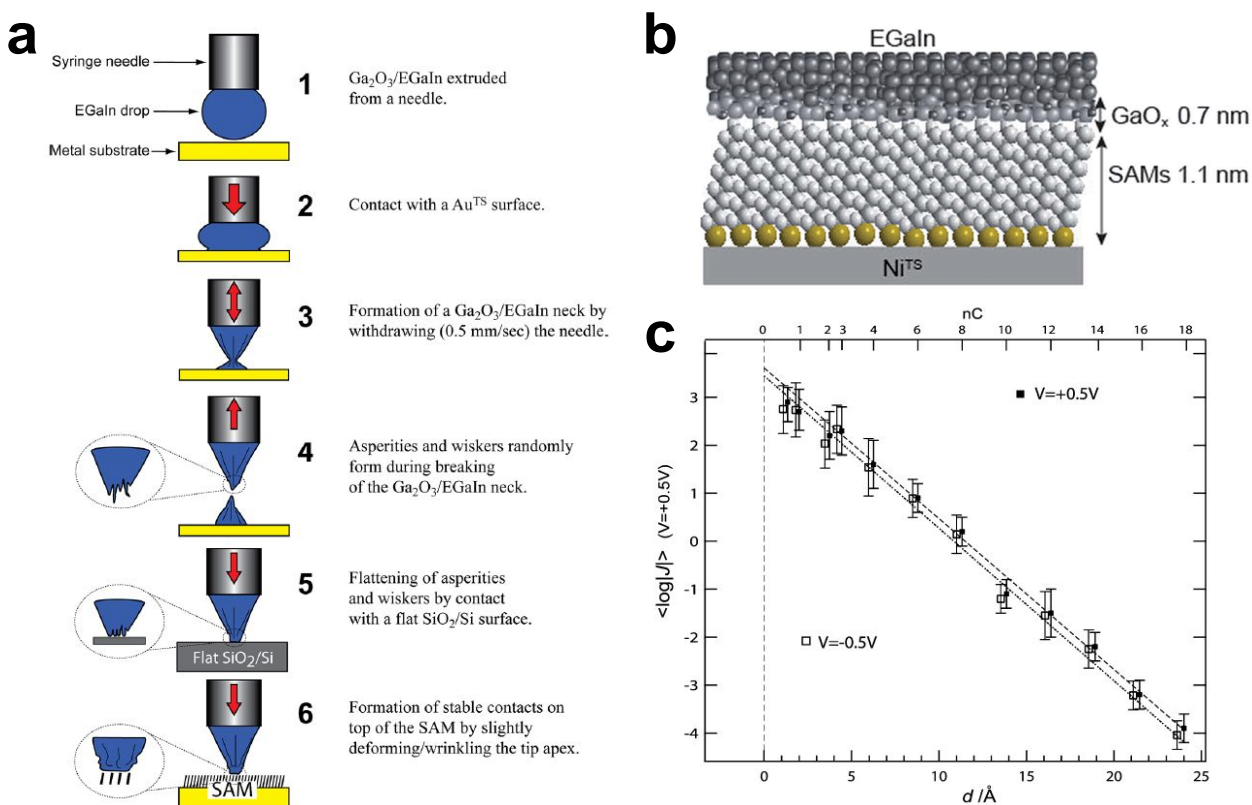


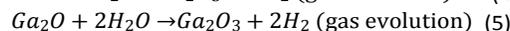
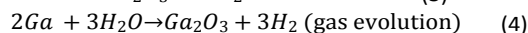
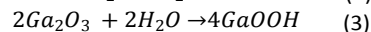
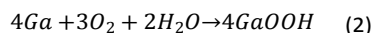
Fig. 5 Forming soft electrode tips for characterizing the electrical properties of thin films. (a) Fabrication and use of Ga₂O₃/EGaIn conical tip electrodes. Reproduced with permission from ref. ⁷². Copyright 2013 American Chemical Society. (b) Schematic of the junction between Ni^{TS}-SAM and a Ga₂O₃/EGaIn electrode. (Ni^{TS}: template-stripped Ni substrate) Reproduced with permission from ref. ⁸². Copyright 2017 Royal Society of Chemistry. (c) Plot of the tunneling current density $\langle \log |J| \rangle$ through SAMs of *n*-alkanethiolates ($n = 1 \sim 18$) as a function of the length d of the tunnel gap established by the alkyl chain. Reproduced with permission from ref. ⁷². Copyright 2013 American Chemical Society.

3 Interface with aqueous environments

GaLMs are directly or indirectly exposed to water from humid or aqueous environments in various applications such as microfluidics, soft electronics, e-skin and wearables, and biomedical devices. Here, the role of water on the interfacial properties of GaLMs and the applications are summarized.

3.1 GaLM in water

When GaLMs are in contact with water, the chemical composition of the oxide skin changes to gallium oxide hydroxide (GaOOH), which is identified by the XRD analysis (Fig. 6(a))⁸⁷. In recent study, it is revealed that H₂ gets produced when GaLMs interact with water⁸⁸. A reaction for converting gallium and gallium oxide to gallium oxide hydroxide and hydrogen by water is proposed in below equations.



GaOOH is less passivating than Ga₂O₃. Also, the mechanical properties of the EGaIn surface oxide skin formed in water (i.e. GaOOH) is weaker than that formed in air (i.e. Ga₂O₃) in Fig. 6(b). The oxide in water showed lower values of the elastic modulus and the yield stress ($G' \sim 1$ N/m, $\sigma \sim 0.1$ N/m) than the oxide formed in the air ($G' \sim 10$ N/m, $\sigma \sim 0.5$ N/m)⁷. While these initial studies were done by adapting bulk rheology tools, more recent measurements using surface rheology tools also produced similar results (Fig. 6(c)). This study compared the elastic modulus, G' , of gallium and its alloys in air and water⁸⁹. In the air, G' values for gallium, EGaIn (75% Ga), and Galinstan (61% Ga) are similar. G' , however, drops significantly in water (relative to air) and the decrease is the largest for gallium. G' increases as the weight percentage of gallium in liquid metal alloy decreases. Such a different mechanical strength of the oxides in air and water affects structural stability of liquid metal droplets. In air, the oxide preserves the shape of micro-scale liquid metal droplet (like a solid shell), whereas, in water, the shapes tend to sag with time.

The conversion of liquid metal to GaOOH can be accelerated by heating⁶. Moderate heating in an aqueous solution converts spherical particles of liquid metal into crystalline rods of GaOOH. The thermal-induced transformation of GaLMs has proven useful for piercing cancer cells⁹⁰ that endocytose liquid metal particles or to destroy films of bacteria⁹¹.

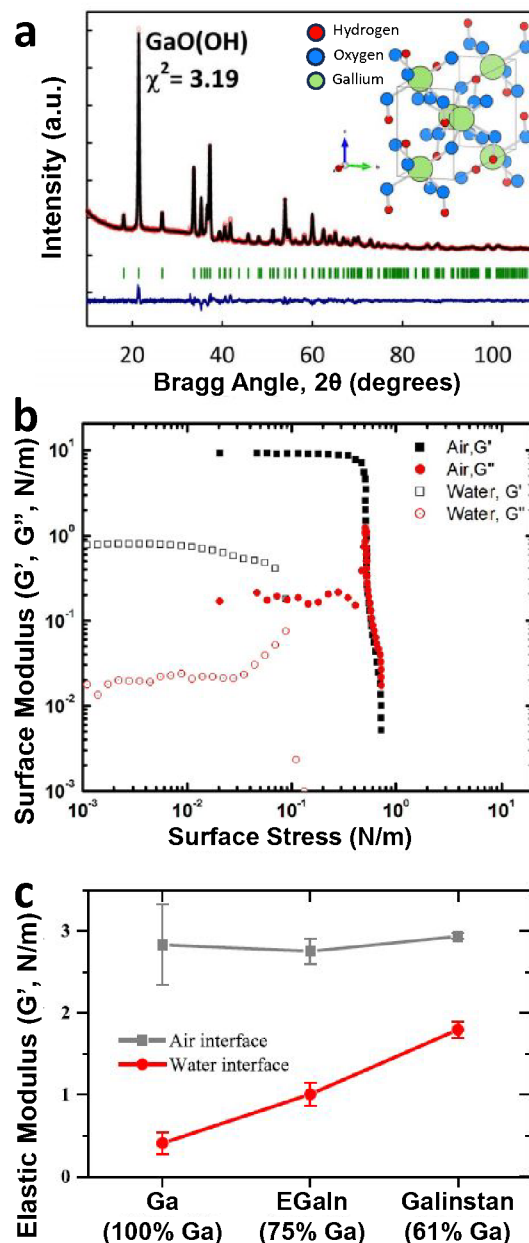
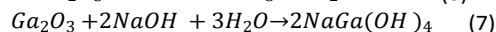


Fig. 6 The role of water on the oxide. (a) XRD data of oxide crystallites formed from the surface GaLMs in water. The inset shows the crystal structure of GaOOH. Reproduced with permission from ref. ⁸⁷. Copyright 2020 American Chemical Society. (b) The surface elastic moduli (G') and the viscous moduli (G'') of the EGaln oxide skin formed in air and water. The values were measured by adopting a bulk rheology tool with the parallel plate geometry to extract these surface moduli. Reproduced with permission from ref. ⁷. Copyright 2014 American Chemical Society. (c) Comparison of the elastic moduli (G') in air and water for gallium (100% Ga), EGaln (75% Ga), and Galinstan (61% Ga). The values were measured by the interfacial rheology tool with the du Noüy ring geometry. Reproduced with permission from ref. ⁸⁹. Copyright 2019 American Chemical Society.

3.2 In acid and base

According to the Pourbaix diagram, the gallium oxide skin is amphoteric and unstable at acidic ($\text{pH} < 3$) or basic ($\text{pH} > 11$) conditions (Fig. 7(a))^{92, 93}. When the gallium oxide is exposed to acidic or basic aqueous solutions, for example, hydrochloric acid

or sodium hydroxide solution, it undergoes a chemical reaction in equations (6) or (7), respectively, to form water-soluble products.



Thus, the gallium oxide on the surface of GaLMs is removed, leaving a smooth metallic surface. In general, sodium hydroxide solution is safer because of its low vapor pressure and tends to remove oxide skin faster than hydrochloric acid solution⁹⁴. The experiments in Figs. 7(b) and (c) show the effect of exposure to acidic and basic solutions on the interfacial behavior of GaLMs^{95, 96}. EGaln initially has non-spherical shapes – a droplet with a conical tip in (b) and line patterns in (c) – due to the oxide skin. Since the oxide skin is chemically removed upon exposure to acid or base solutions, the metal droplet beads up and the narrow metal line is broken and retracts, to minimize the surface area driven by high surface tension of pristine EGaln. The wetting behavior and contact angle of GaLMs depends on pH, which can be used for liquid metal switches and reversible flow systems. Fig. 7(d) shows an environmentally responsive liquid metal switch⁹⁴. First, a Galinstan droplet connects the tungsten lead electrodes in the air, and the LED illuminates. However, when a NaOH solution fills the bath, the metal droplet becomes spherical, disconnecting the circuit and turning off the LED. After the metal droplet is washed with deionized water and dried in the air, the droplet reconnects with the electrodes to turn on the LED.

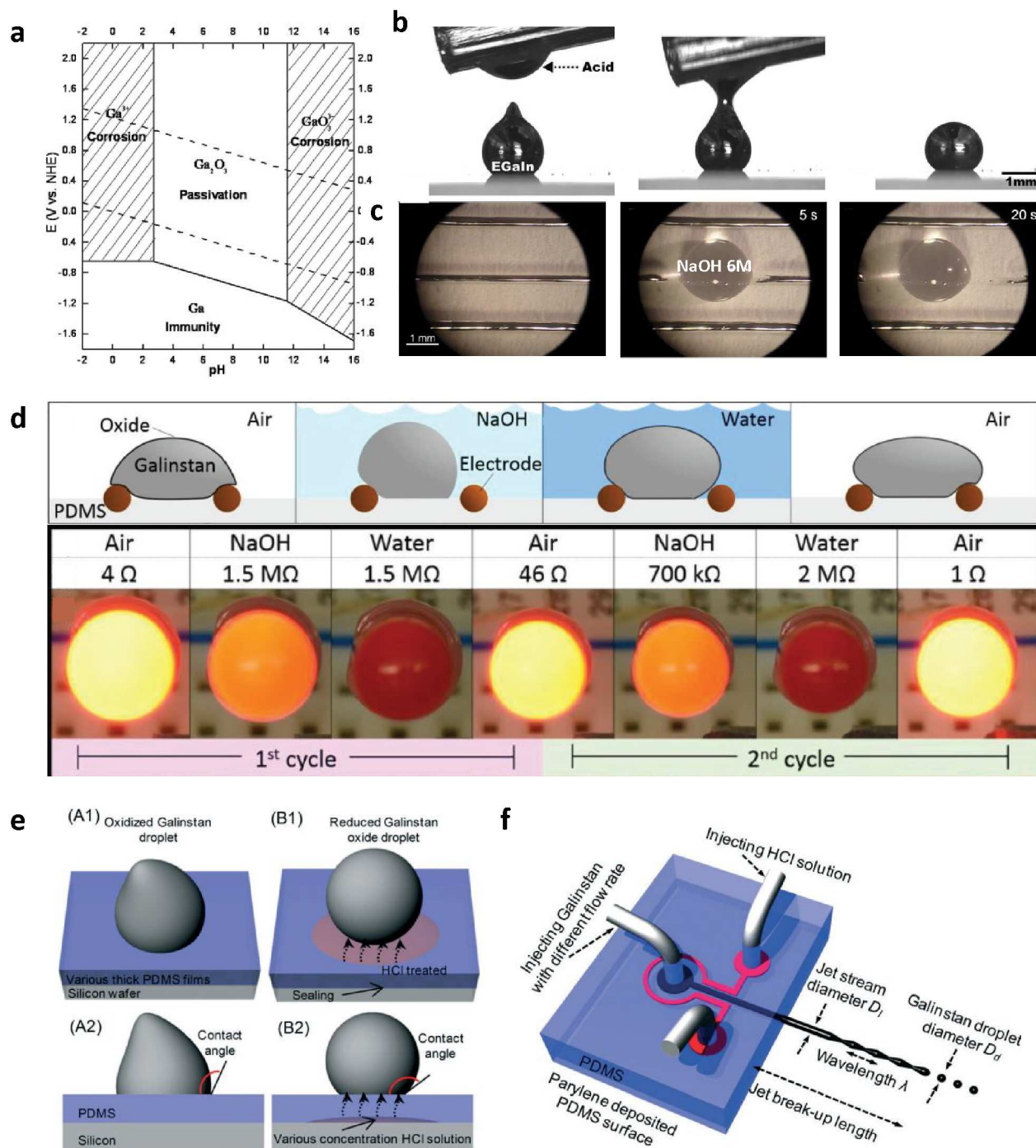


Fig. 7 pH effect on interfacial behavior of GaLMs (a) Potential vs. pH equilibrium diagram of gallium at 25°C. Reproduced with permission from ref. ⁹³. Copyright 2013 The Korean Electrochemical Society. (b) Exposure to acid removes the oxide skin and causes the metal to bead up due to the high surface tension of the bare metal. Reproduced with permission from ref. ⁹⁵. Copyright 2014 American Chemical Society. (c) Chemical method for removing liquid EGaIn circuits using a sodium hydroxide (NaOH) solution. Reproduced with permission from ref. ⁹⁶. Copyright 2017 John Wiley and Sons (d) A liquid metal switch that is repeatedly disconnected and connected depending on environmental stimuli. Reproduced with permission from ref. ⁹⁴. Copyright 2017 John Wiley and Sons. (e) Schematic of oxidized Galinstan droplet and reduced Galinstan droplet using HCl vapor. HCl vapor diffuses through the gas-permeable PDMS. Reproduced with permission from ref. ⁹⁷. Copyright 2014 Royal Society of Chemistry. (f) Schematic of Galinstan-based inkjet printing system. Reproduced with permission from ref. ⁹⁸. Copyright 2016 Royal Society of Chemistry.

It is also possible to effectively remove gallium oxide on the surface of GaLMs using acid vapor instead of the solutions⁹⁹. In acid environment either in liquid or vapor phase, water is formed on the surface of GaLMs as a product by the reaction (6).

Further H₂S gas treatment (> 900 °C) enables the fabrication of two-dimensional semiconducting GaS film with a thickness of 1.5 nm¹⁰⁰. Using a gas-permeable substrate or membrane could provide a safer and more controlled way to expose acid vapor to GaLMs¹⁰¹. For example, PDMS-based coplanar microfluidic channel was designed, where one channel filled with HCl solution was placed parallel to the other^{97, 98}. Diffusion of HCl vapor through the gas-permeable PDMS channel wall removes surface oxide from GaLMs, enabling the effective movement of GaLMs droplet in the channel (Figs.7 (e) and (f)).

3.3 Electrochemical redox reactions

Applying electrical potentials to liquid metal in an aqueous medium is also one of the methods for controlling the interfacial characteristics of GaLMs. As electrical potential is applied to GaLMs, the charge density at the interface of liquid metal changes, leading to change in interfacial energy. This phenomenon is called electrocapillarity, which can be described by the following Lippman's equation^{102, 103}.

$$\gamma = \gamma_0 - \frac{1}{2}c(V - V_{PZC})^2 \quad (8)$$

where γ is the surface tension, γ_0 is the maximum surface tension when $V=0$, c is the capacitance of EDL per unit area, V is the potential difference across the EDL, and V_{PZC} is the potential of zero charge (PZC). When a GaLMs droplet is placed between a cathode and an anode in a channel filled with NaOH solution, the droplet accelerates toward the anode due to the surface tension gradient induced by electrocapillarity (Fig. 8(a))¹⁰⁴. In this case, the metal is not directly attached to an anode and thus, does not oxidize electrochemically (as long as the potential drop is small). Instead, the externally applied field shifts the charges on the surface of the metal toward one side of the droplet, thereby creating asymmetric interfacial tension across the surface of the droplet.

Equation (8) assumes that no electrochemical reactions occur at the interface. Interestingly, when the metal oxidizes electrochemically, the effective tension drops significantly beyond that predicted by Lippman's equation¹⁰⁵. The term 'effective tension' is utilized because the interface contains a thin layer of oxide species and is therefore not a pure liquid-fluid interface. The role of electrochemical oxidation has been reviewed elsewhere and is briefly highlighted here¹⁰⁶⁻¹⁰⁸. Fig. 8(b) shows the change in effective interfacial tension of EGaln via electrochemical oxidation in 1 M NaOH solution⁸. At negative potentials up to low positive potentials (open circuit potential (OCP) < 0.05 V), oxide-free EGaln due to 1 M NaOH electrolyte follows behavior predicted by electrocapillarity. The effects of electrocapillarity are modest in terms of lowering the absolute tension and thus, the metal is a state of high interfacial tension. Conversely, as the oxide electrochemically forms on the surface at elevated positive potential, the effective interfacial tension drops dramatically and EGaln could form an irregular shape, like petals, as shown in Fig. 8(c)¹⁰⁹. The tension can get so low that it can flow through pores¹¹⁰. When a positive potential is applied to the GaLMs exiting a nozzle, the flow of liquid metal changes from a droplet shape to a stable cylindrical stream due to the significant reduction in interfacial tension. The resulting wires can be manipulated using a Lorentz force by placing a magnet behind the wires¹¹¹. At even higher potentials, the oxide thickens, which disrupts the flow of the metal and results in irregular shapes (Fig. 8(d))¹¹².

The gallium oxide deposits on the surface in response to oxidative potentials. Conversely, reductive potentials can remove the oxide layer. This was confirmed by observing that the surface morphology of EGaln in water changes depending on polarities of electrical potentials (Fig. 8(e))¹¹³. Electrochemical oxidation can be used to control the interfacial electrical resistance of GaLMs, that is, increasing the oxide thickness increases the interfacial resistance of GaLMs. This principle can be applied to modulate the conductance of devices based on the GaLM electrodes. Liquid metal electrode-based diodes can be fabricated where the ionic current flows in one direction, using an asymmetric configuration of acidic and basic hydrogel layers (Fig. 8(f))¹¹³. The acidic interface keeps the metal oxide-free (and thus, conductive) at one electrode regardless of the potential, whereas the other electrode surface can switch between resistive (oxidized) and conductive (oxide-free) states depending on the applied potential. The switchable conductance states enable the device to display memristor-like characteristics in which the "1" and "0" correspond to resistive and conductive states due to the presence of absence of oxide (Fig. 8(g))¹¹⁴; this, it is possible to form liquid metal diodes and memory devices that are entirely soft.

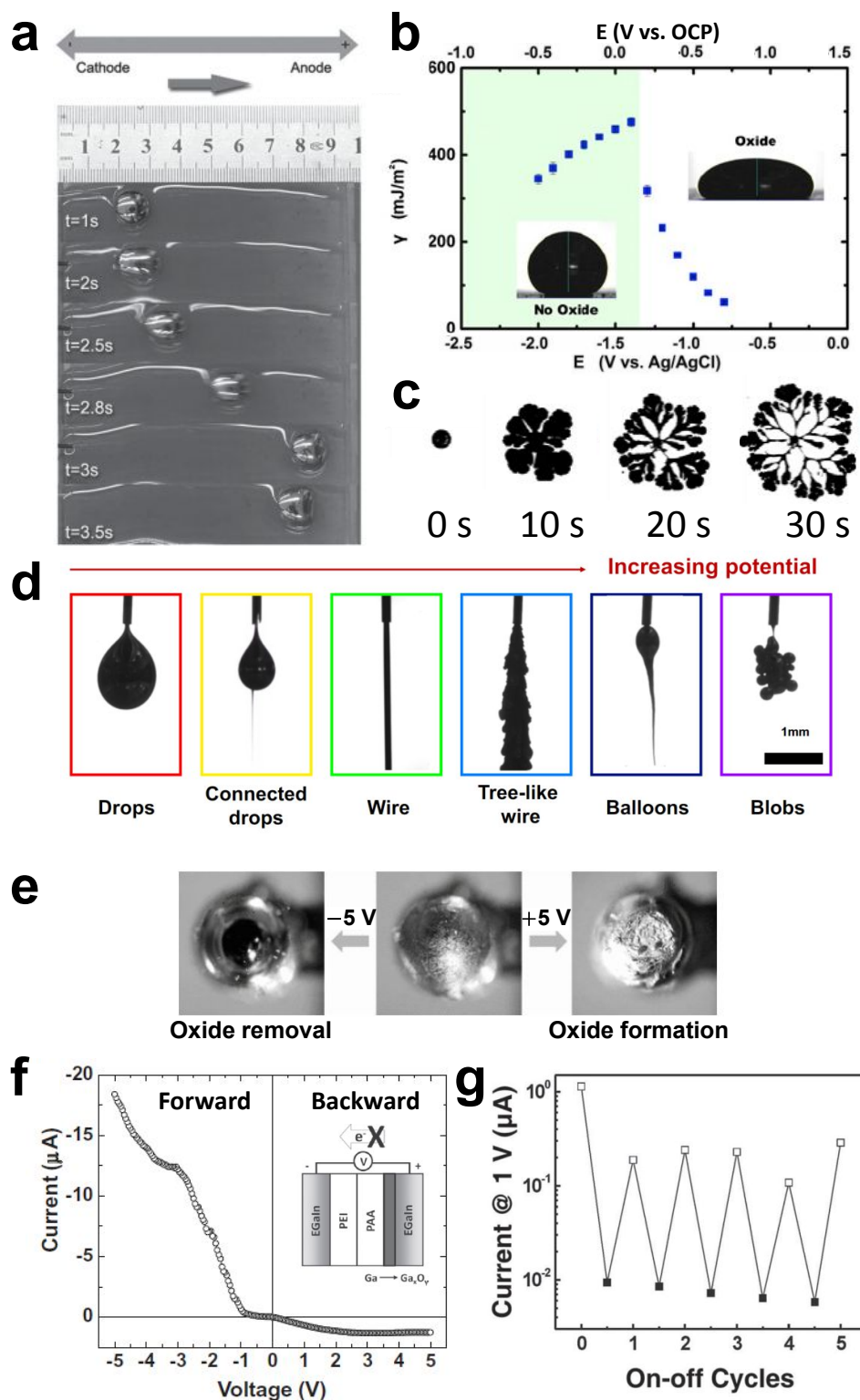


Fig. 8 Electrical manipulation of interfacial tension. (a) Snapshots for Galinstan drop moving in water under an electric field with 12 V DC applied between two electrodes on either side of the droplet, but without directly contacting the droplet. Reproduced with permission from ref. ¹⁰⁴. Copyright 2014 John Wiley and Sons. (b) Effective interfacial tension of EGaln drop as a function of potential measured by sessile drop profile in 1 M NaOH. Electrochemical oxidation causes the tension to drop significantly. Reproduced with permission from ref. ⁸. Copyright 2014 National Academy of Science. (c) The deformation of liquid gallium in 1 M NaOH when 1.3 V is applied. Reproduced with permission from ref. ¹⁰⁹. Copyright 2017 American Physical Society. (d) Morphologies of EGaln liquid metal exiting a nozzle as a function of electric potential. Reproduced with permission from ref.

¹¹². Copyright 2020 National Academy of Science. (e) Top-viewed optical microscope images of EGaIn electrode in water before (middle) and after (left and right) applying biases. (f) Current rectification from the diode with EGaIn electrodes that asymmetrically configured acid (PAA, pH 3)-base (PEI, pH 11) hydrogels. PAA: poly(acrylic acid), PEI: polyethylenimine. Reproduced with permission from ref. ¹¹³. Copyright 2012 John Wiley and Sons. (g) Switching of conductance states of memory devices called ‘memristors’. The switching is based on changes in resistance arising from electrochemical deposition or removal of the oxide skin of the liquid metal. Reproduced with permission from ref. ¹¹⁴. Copyright 2011 John Wiley and Sons.

4 Interface with metals

GaLMs can form amalgams and alloys with other solid metals such as copper, nickel, iron, indium, tin, silver and gold since they have a high affinity for the solid metals. Removing native oxides (using methods discussed in this review) can facilitate metal-metal contact. Adding metals to GaLMs can tune various properties, such as electrical conductivity, thermal conductivity, magnetic polarity, rigidity, wettability, and formability. At the interfaces with solid metals, gallium can destructively diffuse into grain boundaries, form intermetallic compounds, cause intergranular degradation, and weaken the bond between the solid metal atoms even at room temperature^{115–119}. The composition of the reaction product varies depending on the solid metals and reaction conditions. For example, the intermetallic compound between Galinstan and copper substrate was identified as CuGa₂ by XRD as shown in Fig. 9(a)¹²⁰.

However, the presence of a gallium oxide layer can limit the ability of GaLMs to reactively wet other solid metals by acting as a passivating barrier between them. Basic or acidic environments can remove the passivating gallium oxide and induce reactive wetting. This can be seen in Fig. 9(b), which shows that EGaIn droplet spontaneously spreads on the copper substrate in HCl solution without any electric field or external force¹²¹. Using this principle, it is possible to create electrical connections via reactive wetting between EGaIn and micro-device that was composed of tin-plated copper as shown in Fig. 9(c)¹²².

The high affinity of GaLMs for other solid metals enables selective wetting or patterning of liquid metals to regions of a surface coated with patterns of solid metal. Fig. 9(d) depicts the fabrication process of a flexible conductive pattern via selective wetting of GaLMs¹²³. The solid metal, e.g. gold, is patterned on a soft substrate such as PDMS, via photolithography. Then, rolling Galinstan over the pattern generated a soft and stretchable conductive pattern leaving the remaining area clean since the liquid metal selectively wet the solid metal pattern. In this process, however, the corrosion of a thin Cr layer could occur by reacting with the HCl-treated GaLMs, which affects the uniformity of the GaLMs pattern and restricts the high resolution. To address this, an additional Cu layer covered the Au/Cr layer could improve the uniformity, preventing the corrosion issue since the Cu layer does not react with non-oxidizing acids such as HCl and diluted H₂SO₄. As a result, a minimum line width of 2 μm for the Galinstan pattern was achieved¹²⁴.

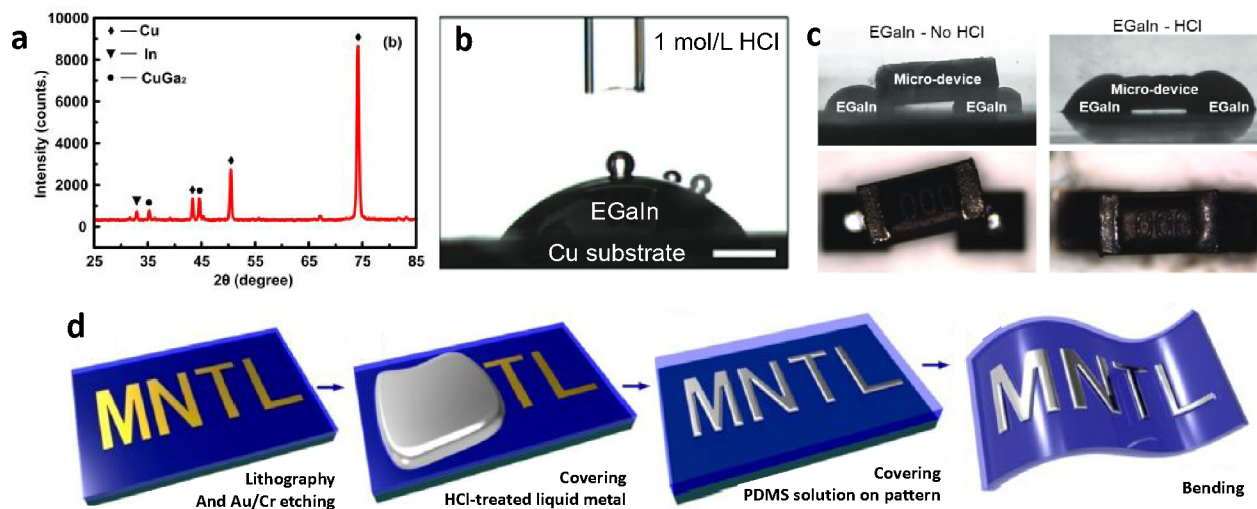


Fig. 9 Interfaces between solid metal and liquid metal. (a) XRD pattern of the reaction product at the interface between Cu and EGaIn. Reproduced with permission from ref. ¹²⁰. Copyright 2018 American Chemical Society. (b) Side-view images of EGaIn droplet reactively wetting a copper plate after HCl solution treatment to remove the native oxides on the metals. Reproduced with permission from ref. ¹²¹. Copyright 2017 John Wiley and Sons. (c) Side-view images a surface-tension driven of connection between EGaIn and a micro-device without (left) and with (right) HCl vapor treatment. Reproduced with permission from ref. ¹²². Copyright 2018 John Wiley and Sons. (d) Fabrication process of the flexible GaLMs pattern via selective wetting between liquid metal and a Au patterned substrate. Reproduced with permission from ref. ¹²³. Copyright 2015 Elsevier.

At certain compositions, adding solid metal particles to GaLMs can produce an amalgam, a semiliquid/semisolid state composite^{125, 126}. The amalgam state of GaLMs and the solid metal particles is soft-solid phase with a good formability, enabling the molding of stable free-standing 3D structures. The properties of amalgams may differ depending on the types of solid metals.

For instance, it was reported that a Cu-EGaIn amalgam mixture showed remarkable improvement in the electrical conductivity and thermal conductivity, and displayed excellent adhesion properties, demonstrating its potential for directly printable electronics (Fig. 10(a))¹²⁷. Due to the high electrical conductivity and excellent deformability, a Cu-EGaIn paste was printed on the skin or 3D surface, which could be used as a computed tomography (CT) assistant localization marker¹²⁸. In addition, the Cu-GaLM mixture has excellent affinity and wettability with GaLM. 3D porous structures made of Cu-EGaIn alloy particles were fabricated, where rapid diffusion of EGaIn liquid metal into the pores was demonstrated, driven by capillary force (Fig. 10(b))¹²⁹.

Printing of a suspension of solid particles can be challenging due to particles settling. Nevertheless, concentrations of Cu and Ga can be combined to form a temporary paste that can be molded or printed at room temperature, and then ultimately harden into a solid CuGa_2 intermetallic with a melting point of 540 °C; this allows solid metals to be printed at room temperature¹³⁰. To address the printability issue, liquid metal may be used to form ‘bridges’ between Cu particles to form a ‘metallic gel’ network that can be printed at room temperature. The resulting parts are metallically conductive and can even change shape after printing to enable so-called 4D printing¹³¹.

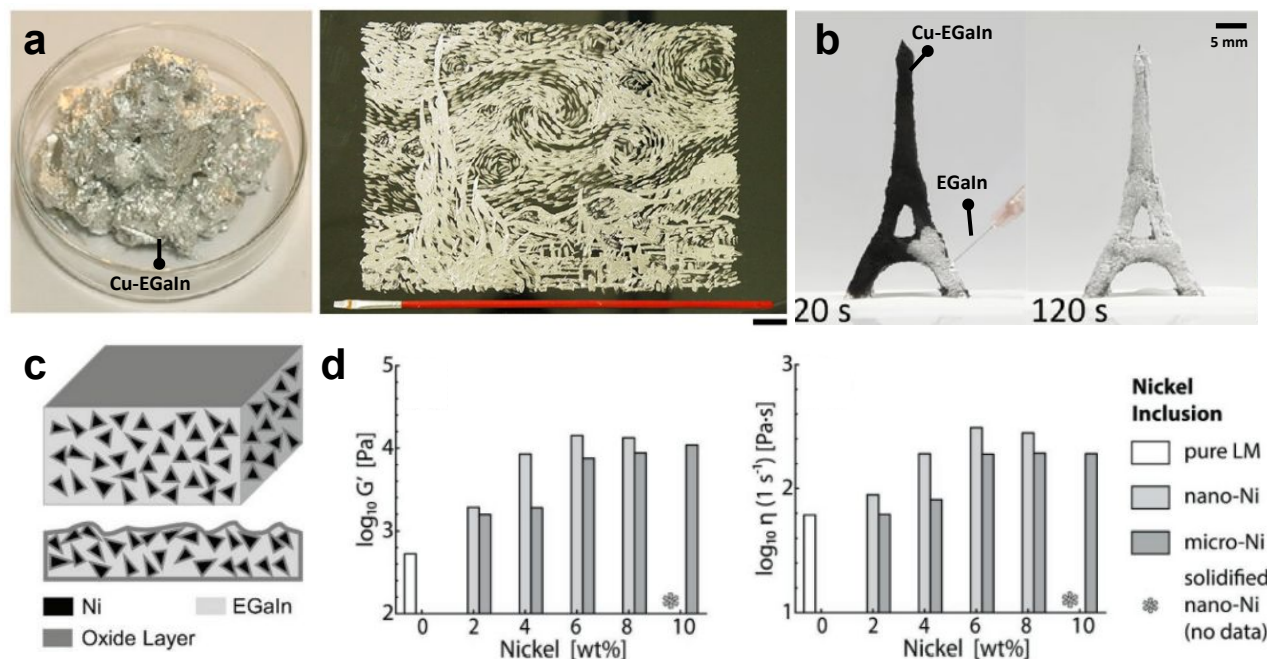


Fig. 10 Interactions of liquid metal with solid metal particles. (a) Cu-EGaIn amalgam with $\Phi = 15\%$ (left) and painting with a brush using Cu-EGaIn amalgam (right). Φ is defined as $mass_{Cu}/mass_{EGaIn}$. Reproduced with permission from ref. ¹²⁷. Copyright 2017 American Chemical Society. (b) Spontaneous diffusion of EGaIn into 3D porous structure made of Cu-EGaIn particles. The EGaIn liquid metal penetrated and diffused within the Cu-EGaIn-based structure driven by capillary force. Reproduced with permission from ref. ¹²⁹. Copyright 2020 American Chemical Society. (c) The schematic of the internal structure of Ni-EGaIn. Ni particles were wrapped by the gallium oxide layer. Reproduced with permission from ref. ¹³². Copyright 2019 John Wiley and Sons. (d) The plots of the average elastic modulus (G') (left) and viscosity (η) (right) for EGaIn-Ni particles as the function of nickel weight fraction from 2–10 wt%. Reproduced with permission from ref. ¹³³. Copyright 2018 John Wiley and Sons.

Particles that are not metallic or those that are coated with a very stable layer of oxide do not readily mix with liquid metal. In such cases, it is possible to entrain the particles into the liquid metal by stirring in the presence of the native oxide, which wraps around the particles to allow them to enter the metal, such as nickel and tungsten^{132, 134–136}. Superficially, this process is analogous to endocytosis. For example, Ni-EGaIn amalgam, in which the gallium oxide layer wrapped around the Ni particles and gave scaffold-like support for the dispersed particles (Fig. 10(c)), exhibits an increase in elastic modulus and viscosity (Fig. 10(d))¹³³. Furthermore, accelerated oxidation by continuous stirring reduces fluidity as well as surface tension, enabling GaLMs based amalgams to be deposited on various substrates, such as Eco-flex, PMA, or skin. This conductive paste can be applied to wearable, flexible electronics and e-skin devices for healthcare^{127–129, 132, 134, 137–139}.

Even though Ga is diamagnetic, it can be imparted with magnetic properties by incorporating magnetic particles. For example, magnetic responsive Fe-Ga particles can form by combining iron particles with liquid gallium^{140, 141}. These gallium-coated iron particles can be dispersed in uncured elastomer and assembled into soft and stretchable conductive microwires in response to magnetic fields. Additionally, ferromagnetic neodymium–iron–boron (NdFeB) microparticle can be aligned within GaLMs matrix under a magnetic field, resulting in the solid, putty-like amalgam having the corresponding magnetic polarity^{137, 142}. Based on paper coated with the ferromagnetic NdFeB-GaLMs film, an inchworm-like actuator that responds to the magnetic field with a crawling speed of 29.7 mm s^{-1} was demonstrated (Fig. 11(a))¹³⁷. The magnetic-responsive soft robot was also

fabricated by mixing and magnetizing NdFeB particles within Ga and embedding the amalgam in the PDMS shell. As an example of programmable motions, the soft robot showed grasping and delivering a target as shown in Fig. 11(b)¹⁴².

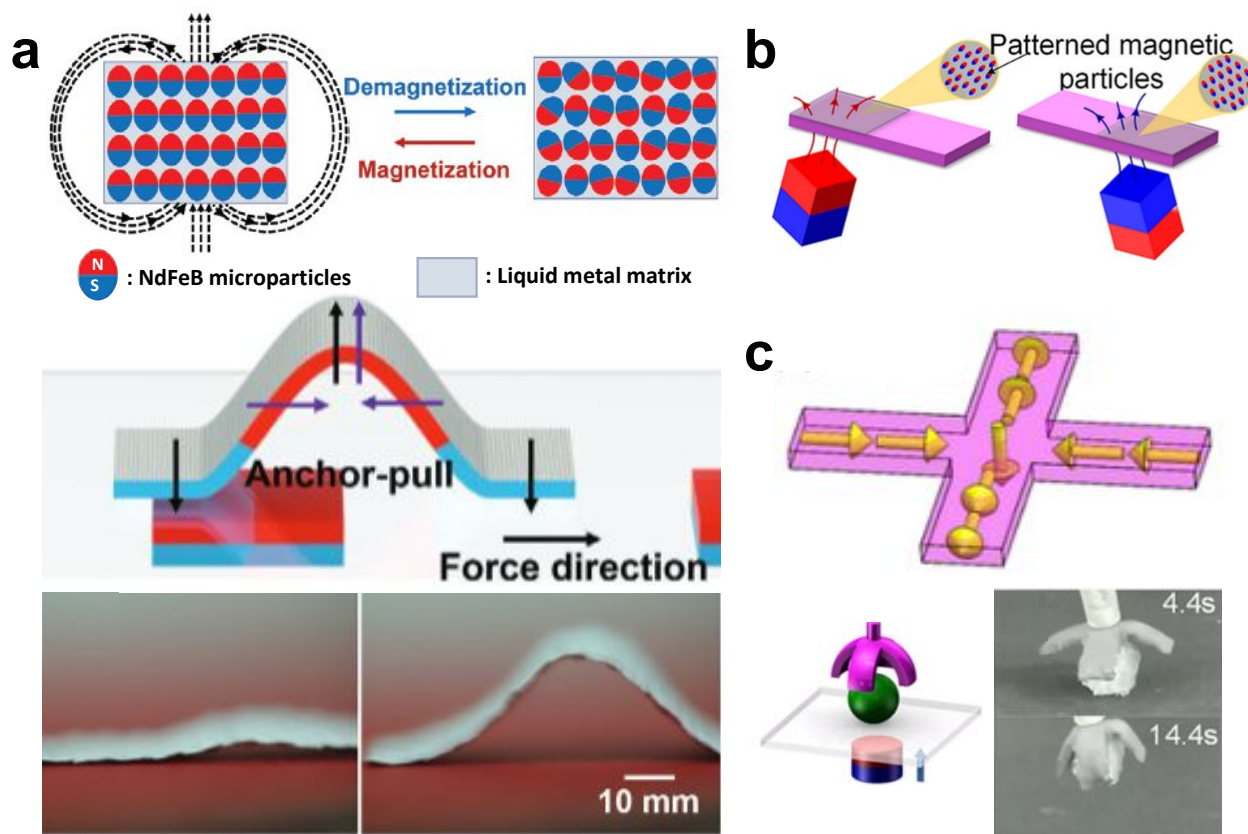


Fig. 11 Incorporating magnetic particles into liquid metal. (a) Magnetization of NdFeB particles in GaLMs matrix under the magnetic field (upper) and the magnetic-responsive actuator based on NdFeB-GaLMs-coated paper (lower). Reproduced with permission from ref. ¹³⁷. Copyright 2020 John Wiley and Sons. (b) Magnetic grasper by aligning NdFeB particles within Ga/PDMS matrix. (c) Magnetization profile and grasping action. Reproduced with permission from ref. ¹⁴². Copyright 2022 IEEE.

5 Interface with non-metallic materials

GaLMs without oxides typically exhibit poor adhesion on non-metallic surfaces, such as polymer substrates. With the oxide, the adhesive behavior is complex. The term 'wetting' is often misused; if the oxide is present, then droplets 'adhere' to surfaces. Metrics like static contact angle are effectively meaningless because the oxide does not allow the metal to flow freely, which is a requisite for using contact angles. If the droplet is advanced (i.e. volume increasing) on a surface, it adheres to seemingly all smooth solid surfaces¹⁴³. If the surfaces are rough, the oxide does not adhere¹⁴⁴⁻¹⁴⁶, which provides a route to create non-stick surfaces. The behavior of the oxide-coated metal on smooth surfaces is complicated: If a droplet of metal is merely contacted with a surface, it may or may not adhere. First, the oxide on the metal may have roughness from wrinkles that prevents good contact, which helps explain why advancing helps promote adhesion. Second, the oxide should interact favorably with the surface to promote adhesion. Since the oxide is hydrophilic and hydroxyl terminated, it naturally adheres to hydrophilic surfaces such as polymethacrylate (PMA)^{147, 148}, poly(3,4-ethylenedioxythiophene):poly(4-styrenesulfonate) (PEDOT:PSS)¹⁴⁹, polyvinyl alcohol (PVA)^{150, 151}, and poly(2-hydroxyethyl acrylate) (PHEA)¹⁵². The oxide coated metal adheres less-well to silicones (hydrophobic), but the adhesion improves with plasma treatment (hydrophilic)⁶⁷. As an example, Fig. 12(a) shows that PMA acts as the intermetallic adhesive layer for EGaIn coating due to the adhesion between PMA and gallium oxide¹⁴⁷. In a recent study, the excellent adhesion of Galinstan on PEDOT:PSS film was observed, which was attributed to the strong interaction between Ga₂O₃ and PEDOT:PSS, as evidenced by a new peak corresponding to the PEDOT:PSS-Ga(III) complex in the XPS spectrum (Fig. 12(b))¹⁴⁹.

The surface of GaLMs without oxide could present a catalytic platform for carbon material growth since they promote the formation of C-C bonds¹⁵³⁻¹⁵⁵. Moreover, their ultrasmooth surface and the absence of interfacial forces allow for facile exfoliation of products^{156, 157}. A recent study reports that the selective synthesis of propylene using liquid gallium as a solvent for catalytic reactions, where the Ga matrix provides a surface for active reconfiguration¹⁵⁸.

Studies have explored the interaction between GaLMs (with native oxides) and carbon materials such as graphene, graphite, and carbon nanotubes. Chemically oxidizing CNTs by acid treatment allows for stable adhesion between CNTs and GaLMs. An oxygen functional group on the oxidized CNTs can enhance the interaction between CNTs and GaLMs, resulting in a robust attachment to the EGaIn surface even under deformation¹⁵⁹.

The transformation of GaLMs through contact with graphite in an alkaline solution has also been reported¹⁶⁰. Upon contact with graphite in alkaline solution, a potential drop at the interface of GaLMs and graphite leads to electron transfer from GaLMs to graphite (Fig. 12(c)). As a result, the oxidation of GaLMs occurs, which significantly decreases its surface tension and causes a transformation to a flat film shape.

GaLMs could form composites with non-metallic particles such as graphene oxide (GO), graphite, diamond, and silicon carbide¹⁶¹⁻¹⁶⁴. For the successful formation of a composite of non-metallic fillers and GaLMs, gallium oxide is critical (Fig. 12(d))¹⁶⁵, as discussed in the previous section 2.3. It forms a filler-gallium oxide-GaLMs interaction, which helps enable incorporation of filler particles. The potential applications and performance of the GaLMs composite with carbon-based fillers are determined by the properties of the fillers. The inclusion of carbon materials improves the mechanical strength, processability and electrical and thermal properties, enabling the creation of free-standing structures, 3D printing patterns, and thermal interface materials (TIMs). CNT-EGaIn composites exhibit enhanced modulus and mechanical stability, enabling it 3D printing with high resolution (5 μm)¹⁶⁶. Composites containing GO demonstrate excellent processability, and the composites containing diamond or reduced-GO exhibited high thermal conductivity of range 104 ~ 126 W/m·K compared to pure liquid metal (Ga/EGaIn/Galinstan) of range 25 ~ 30 W/m·K¹⁶¹. Thermally and electrically conductive graphene networks in gallium exhibit high thermal conductivity (44.6 W/m·K) and electrical conductivity (8.3 S/ μm), making it ideal for use as TIMs¹⁶⁷.

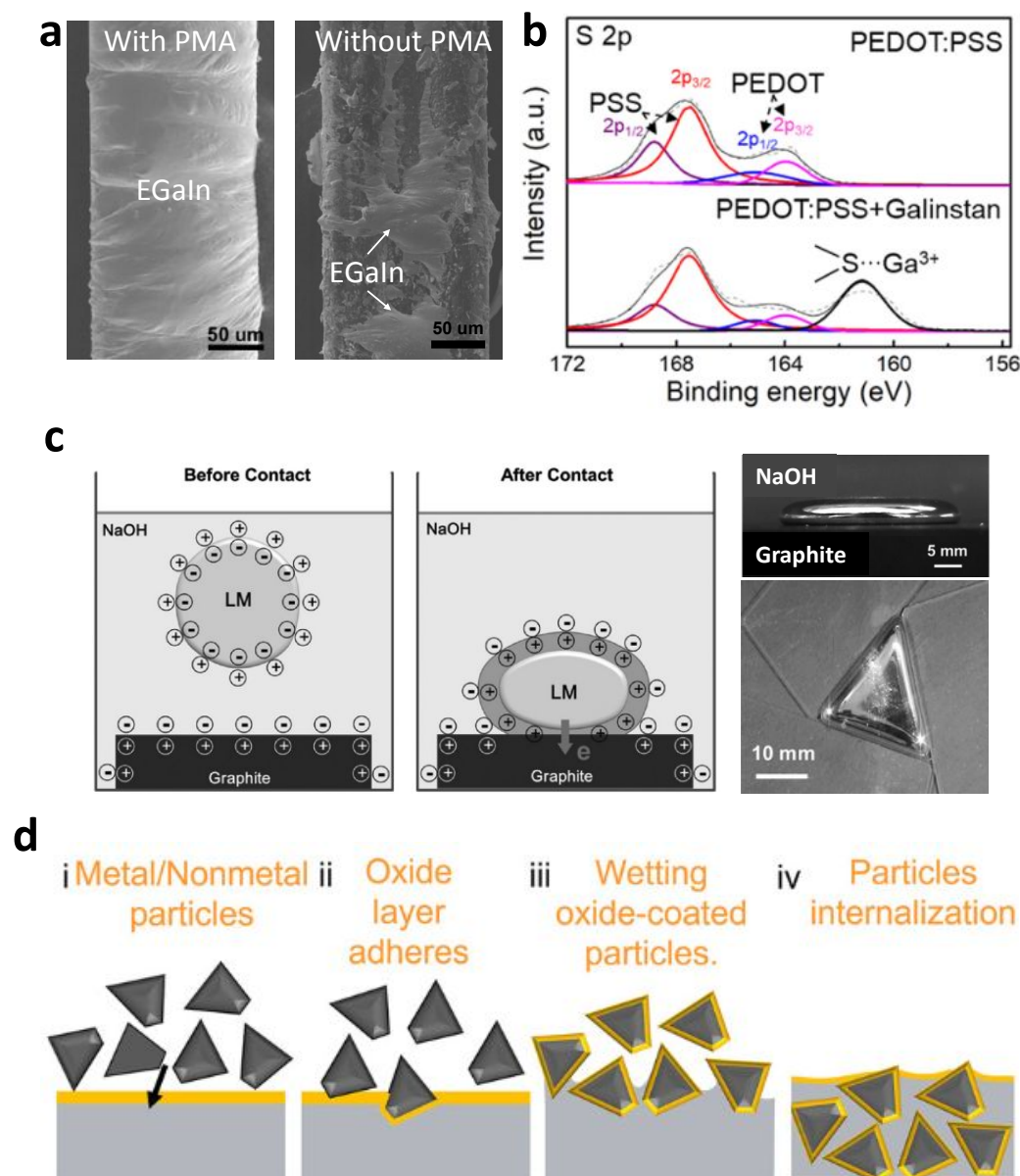


Fig. 12 Interactions of GaLMs with non-metallic materials. (a) SEM images of the conductor fiber covered by EGaIn with PMA intermediate layer (left) and without PMA (right). Reproduced with permission from ref. ¹⁴⁷. Copyright 2020 American Chemical Society. (b) S 2p XPS spectrum of PEDOT:PSS before and after mixing with Galinstan. Reproduced with permission from ref. ¹⁴⁹. Copyright 2023 Elsevier. (c) Flattening deformation of Galinstan driven by electrochemical oxidation upon contacting with graphite in NaOH. The gallium oxide layer is formed on a Galinstan droplet due to the negative potential drop from Galinstan to graphite. Reproduced with permission from ref. ¹⁶⁰. Copyright 2016 John Wiley and Sons. (d) Schematic showing the fabrication of GaLMs composites with carbon-based fillers. Reproduced with permission from ref. ¹⁶⁵. Copyright American Chemical Society.

6 Effect of surface topography on interfacial characteristics of GaLMs

Surfaces that are rough and textured affect interfacial adhesion / wetting of GaLMs with / without the oxide. We focus initially on the metal with the oxide. Like other liquids, GaLMs have two states on a rough surface: Wenzel and Cassie-Baxter states, which is, largely dictated by the roughness dimensions. When the dimensions of surface roughness are small, e.g., in the nanometer to tens of micrometer scales, GaLM with the oxide skin is in the Cassie-Baxter state due to the formation of an air gap between the solid oxide and valleys of the roughness, as shown in Fig. 13(a)^{168, 169}. The solid oxide skin prevents the liquid metal from intruding the valleys, thus GaLMs with the oxide are difficult to adhere to rough surfaces. The Wenzel state occurs when

GaLMs completely fill the micro-structures of surface, when the roughness scale of substrate is large, e.g., in the hundreds of micrometer to millimeter (Fig. 13(b)).

The significant stickiness of gallium oxide on almost any substrate makes GaLMs challenging to handle and control reversibly. This can be addressed by introducing nano/micro roughness to the surfaces where GaLMs do not adhere in the Cassie-Baxter state. Methods for forming nano/micro roughness on a surface include nanoparticles coating^{144, 145, 170}, laser writing^{171, 172}, and soft lithography^{169, 173}. For instance, glass substrates coated with silica nanoparticles form a rough surfaces where GaLMs do not adhere and leave no oxide residue when detached (Fig. 13(c)). Patterns of nano/micro-structured surfaces enable EGaIn patterning by selective adhesion. Such rough coatings can also be used on the inside of channels and 3D printed parts to prevent adhesion¹⁴⁵.

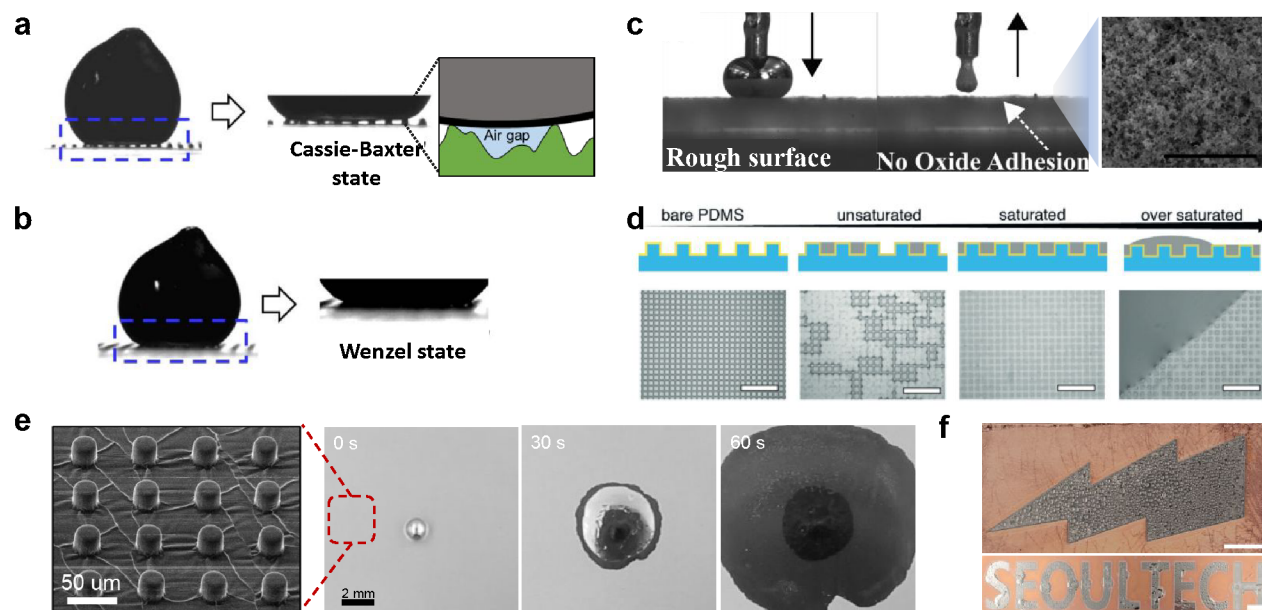


Fig. 13 The role of surface roughness on interfacial adhesion and wetting of liquid metal. (a-b) The side-view images of Galinstan droplets in two wetting states: (a) Cassie-Baxter state and (b) Wenzel state. Reproduced with permission from ref. ¹⁶⁹. Copyright 2013 IEEE. (c) The side view images of EGaIn droplet contacting the rough surface. The drop completely withdraws with no residual oxide on the rough surface. The SEM image shows the rough surface coated with silica nanoparticles. Scale bar is 2 μm . Reproduced with permission from ref. ¹⁴⁴. Copyright 2018 American Chemical Society. (d) Schematics and optical images of gallium film deposited on a microstructured substrate (Au/PDMS). Scale bars are 30 μm . Reproduced with permission from ref. ¹⁷⁴. Copyright 2018 John Wiley and Sons. (e) Imbibition-induced spontaneous wetting of EGaIn on a micro-structured metallic surface in the presence of HCl vapor. (f) EGaIn patterning via imbibition-induced selective wetting. Scale bars are 5 mm. Reproduced with permission from ref. ¹⁷⁵. Copyright 2022 Springer Nature.

In the absence of the gallium oxide skin, the formation of a thin film of GaLMs is challenging due to their high surface tension. However, this issue can be addressed by adopting a micro-topography on the liquid metal-favorable surface like metals. Oxide-free GaLMs can be deposited by physical vapor deposition. When gallium is deposited by thermal evaporation on microstructured gold substrates, smooth and homogenous film of gallium forms by imbibition which is a capillary-driven transport process where the liquid invades a textured surface (Fig. 13(d))¹⁷⁴. Introducing HCl vapor can trigger the enhanced wetting by removing the oxide skin of GaLMs. EGaIn can wet micro-structured copper surfaces in the presence of acid vapour to keep the metal oxide free (Fig. 13(e))¹⁷⁵. EGaIn reactively wets the copper and fills into the topography by ‘imbibition’. The patterning of the liquid metal is also possible because the liquid metal selectively wets along the region with the micro-structures (Fig. 13(f)). The unique wetting characteristics of GaLMs enables control of the film thickness as well as spontaneous coating/patterning of the liquid metal on various substrates for stretchable electronics and other emerging applications.

7 Closing Remarks and Outlook

This review discusses the interfacial properties and behavior of GaLMs in various environments and possible applications based on them. In air, by the Cabrera-Mott (CM) oxidation mechanism, a self-passivating gallium oxide skin forms on the surface of GaLMs. The presence of a solid oxide on the surface changes the interfacial chemistry from metallic to oxide-terminated while adding a mechanical (solid) skin that encases the metal. The oxide skin allows the metal to form stable shapes by injection into micro-channels, 2D/3D printing, or forming soft electrode tips. In water, the composition of the oxide skin changes to GaOOH with lower mechanical strength and poor passivation. The thickness of the oxide skin in the aqueous environment can be

controlled by pH or electric bias, which has been adopted for modulating interfacial resistance or surface tension in many applications previously reported, such as diodes, memristors, and electric switches. When contacting most metals, GaLMs have a good wettability. When mixed with metal particles, GaLMs become a soft semi-solid amalgam with good formability, enabling stable free-standing 3D shapes. GaLMs without oxides generally exhibit poor adhesion on non-metallic surfaces. In the presence of oxide skin, the adhesive behavior of GaLMs is complicated and depends on surface roughness and how the metal contacts the surface. For inclusion of non-metallic fillers in GaLMs, the gallium oxide layer is important to form a stable interface between GaLMs and the fillers. Surface topography significantly affects the adhesive characteristic of GaLMs featuring surface oxides. Introducing nano- and micro-scale roughness on a surface prevents GaLMs from wetting or adhering on the surface. On the other hand, GaLMs exhibit rapid, spontaneous spreading on the textured metallic surface because of the enhanced wetting induced by imbibition.

GaLMs have been demonstrated in the literature as having applications in a variety of fields, including electronics, sensors, microfluidics, energy, catalysts, and biomedical engineering, where the liquid metals are in contact with various substances in gas, liquid, or solid phase as mentioned above. As the effort to discover and exploit the characteristics of the metals and their interfaces has been increasing, it is critical to understand the interfacial characteristics of the liquid metals. The systematic studies on the interface of the metals would include understanding the meaning of contact angles and their hysteresis, wetting, and adhesion. The surface oxide that GaLMs have in most environments is a few nanometers thick, solid-phase film and tends to stick to or pin on a surface. The oxide causes abnormal interfacial behaviors of GaLMs different from those of common liquids, depending on the presence or absence of the oxide or its composition. Surprisingly, it is easy to find that many papers carry out routine interface analysis methods (such as contact angles) and discussions without careful consideration on the hetero-phase interface of GaLMs. For better analysis and understanding of the interfacial behaviors of the liquid metal, a rational standard procedure should be established according to the surface oxide conditions.

In-depth studies on the oxide of the liquid metal should promote novel technologies and applications as the nanometer-thick oxide skin dominates the interfacial properties of the liquid metal. The electrical properties of the surface oxide, such as electrical conductivity, band gap, and permittivity, need to be investigated depending on its thickness and composition which could be varied in response to its environment. The composition of the oxide versus depth would also be the interest to fundamental and nano-scale research. To broaden the potential applications for liquid metals, further research is needed to enhance their stability under various challenging conditions, including extremes of temperature as well as acidic or basic environment. Rational engineering of the surface chemistry will allow GaLMs to be more actively employed for energy harvesting and storage, catalysts, biological research and more. Moreover, it would be possible to design and fabricate new types of composites of the liquid metals with other materials like polymers, elastomers, and gels with previously unreported procedures and compositions. The novel composites would further expand the possibilities of liquid metals and contribute to inventing their more applications, such as soft robotics and actuators.

Author contributions

J.-H. Kim, conceptualization, investigation, visualization, writing-original draft & editing; S. Kim conceptualization; M. D. Dickey, conceptualization, writing-review & editing; J.-H. So, conceptualization, supervision, writing-review & editing; H.-J. Koo, conceptualization, supervision, writing-review & editing

Conflicts of interest

There are no conflicts to declare.

Acknowledgements

This work has been supported by Basic Science Research Programs funded by the Ministry of Education (NRF-2021R1A6A1A03039981) and the Korea Environment Industry & Technology Institute (KEITI) funded by the Korea Ministry of Environment (MOE) (No. 2022002980003). M.D.D. is grateful for support from the National Science Foundation Division of Civil, Mechanical, and Manufacturing Innovation grant 2032409.

References

1. C. Dodd, *Proc. Phys. Soc. London, Sect. B*, 1950, **63**, 662.
2. C. Karcher, V. Kocourek and D. Schulze, 2003.
3. D. Morales, N. A. Stoute, Z. Yu, D. E. Aspnes and M. D. Dickey, *Appl. Phys. Lett.*, 2016, **109**, 091905.
4. J. Ma, F. Krisnadi, M. H. Vong, M. Kong, O. M. Awartani and M. D. Dickey, *Adv. Mater.*, 2023, **35**, 2205196.

5. A. Zavabeti, J. Z. Ou, B. J. Carey, N. Syed, R. Orrell-Trigg, E. L. Mayes, C. Xu, O. Kavehei, A. P. O'Mullane, R. B. Kaner, K. Kalantar-Zadeh and T. Daeneke, *Science*, 2017, **358**, 332-335.
6. Y. Lin, Y. Liu, J. Genzer and M. D. Dickey, *Chem. Sci.*, 2017, **8**, 3832-3837.
7. M. R. Khan, C. Trlica, J.-H. So, M. Valeri and M. D. Dickey, *ACS Appl. Mater. Interfaces*, 2014, **6**, 22467-22473.
8. M. R. Khan, C. B. Eaker, E. F. Bowden and M. D. Dickey, *PNAS*, 2014, **111**, 14047-14051.
9. S. Handschuh-Wang, L. Zhu, T. Gan, T. Wang, B. Wang and X. Zhou, *Appl. Mater. Today*, 2020, **21**, 100868.
10. Y. Ding, M. Zeng and L. Fu, *Matter*, 2020, **3**, 1477-1506.
11. K. Akyildiz, J.-H. Kim, J.-H. So and H.-J. Koo, *J. Ind. Eng. Chem.*, 2022, **116**, 120-141.
12. K. Y. Kwon, V. K. Truong, F. Krisnadi, S. Im, J. Ma, N. Mehrabian, T.-i. Kim and M. D. Dickey, *Adv. Intell. Syst.*, 2021, **3**, 2000159.
13. M. D. Dickey, R. C. Chiechi, R. J. Larsen, E. A. Weiss, D. A. Weitz and G. M. Whitesides, *Adv. Funct. Mater.*, 2008, **18**, 1097-1104.
14. F. Scharmann, G. Cherkashinin, V. Breternitz, C. Knedlik, G. Hartung, T. Weber and J. Schaefer, *Surf. Interface Anal.*, 2004, **36**, 981-985.
15. M. Regan, H. Tostmann, P. S. Pershan, O. Magnussen, E. DiMasi, B. Ocko and M. Deutsch, *Phys. Rev. B*, 1997, **55**, 10786.
16. C. Su, P. Skeath, I. Lindau and W. Spicer, *Surf. Sci.*, 1982, **118**, 248-256.
17. L. Cademartiri, M. M. Thuo, C. A. Nijhuis, W. F. Reus, S. Tricard, J. R. Barber, R. N. S. Sodhi, P. Brodersen, C. Kim, R. C. Chiechi and G. M. Whitesides, *J. Phys. Chem. C*, 2012, **116**, 10848-10860.
18. D. R. Lide, *CRC handbook of chemistry and physics*, CRC press, 2004.
19. S. Zhao, J. Zhang and L. Fu, *Adv. Mater.*, 2021, **33**, 2005544.
20. N. J. Morris, Z. J. Farrell and C. E. Tabor, *Nanoscale*, 2019, **11**, 17308-17318.
21. Z. J. Farrell and C. Tabor, *Langmuir*, 2018, **34**, 234-240.
22. H. Song, T. Kim, S. Kang, H. Jin, K. Lee and H. J. Yoon, *Small*, 2020, **16**, 1903391.
23. L. Ren, J. Zhuang, G. Casillas, H. Feng, Y. Liu, X. Xu, Y. Liu, J. Chen, Y. Du, L. Jiang and S. X. Dou, *Adv. Funct. Mater.*, 2016, **26**, 8111-8118.
24. S.-Y. Tang, D. R. Mitchell, Q. Zhao, D. Yuan, G. Yun, Y. Zhang, R. Qiao, Y. Lin, M. D. Dickey and W. Li, *Matter*, 2019, **1**, 192-204.
25. S. Liu, S. N. Reed, M. J. Higgins, M. S. Titus and R. Kramer-Bottiglio, *Nanoscale*, 2019, **11**, 17615-17629.
26. J. Cutinho, B. S. Chang, S. Oyola-Reynoso, J. Chen, S. S. Akhter, I. D. Tevis, N. J. Bello, A. Martin, M. C. Foster and M. M. Thuo, *ACS nano*, 2018, **12**, 4744-4753.
27. A. Martin, W. Kiarie, B. Chang and M. Thuo, *Angew. Chem.*, 2020, **132**, 360-365.
28. Y. Lin, J. Genzer and M. D. Dickey, *Adv. Sci.*, 2020, **7**, 2000192.
29. S. Hardy, *J. Cryst. Growth*, 1985, **71**, 602-606.
30. D. Zrnic and D. Swatik, *J. Less-Common Met.*, 1969, **18**, 67-68.
31. V. Y. Prokhorenko, V. V. Roshchupkin, M. A. Pokrasin, S. Prokhorenko and V. Kotov, *High Temp.*, 2000, **38**, 954-968.
32. I. D. Joshipura, H. R. Ayers, C. Majidi and M. D. Dickey, *J. Mater. Chem. C*, 2015, **3**, 3834-3841.
33. Y. Lin, O. Gordon, M. R. Khan, N. Vasquez, J. Genzer and M. D. Dickey, *Lab Chip*, 2017, **17**, 3043-3050.
34. Y. Huang, Y. Wang, L. Xiao, H. Liu, W. Dong and Z. Yin, *Lab Chip*, 2014, **14**, 4205-4212.
35. M. Kubo, X. Li, C. Kim, M. Hashimoto, B. J. Wiley, D. Ham and G. M. Whitesides, *Adv. Mater.*, 2010, **22**, 2749-2752.
36. S. Cheng, Z. Wu, P. Hallbjorner, K. Hjort and A. Rydberg, *IEEE Trans. Antennas Propag.*, 2009, **57**, 3765-3771.
37. M. Rashed Khan, G. J. Hayes, J.-H. So, G. Lazzi and M. D. Dickey, *Appl. Phys. Lett.*, 2011, **99**, 013501.
38. J. H. So, J. Thelen, A. Qusba, G. J. Hayes, G. Lazzi and M. D. Dickey, *Adv. Funct. Mater.*, 2009, **19**, 3632-3637.
39. S. Cheng, A. Rydberg, K. Hjort and Z. Wu, *Appl. Phys. Lett.*, 2009, **94**, 144103.
40. S. Cheng and Z. Wu, *Lab Chip*, 2010, **10**, 3227-3234.
41. C. Majidi, R. Kramer and R. Wood, *Smart Mater. Struct.*, 2011, **20**, 105017.
42. Y.-L. Park, C. Majidi, R. Kramer, P. Bérard and R. J. Wood, *J. Micromech. Microeng.*, 2010, **20**, 125029.
43. Y.-L. Park, B.-R. Chen and R. J. Wood, *IEEE Sens. J.*, 2012, **12**, 2711-2718.
44. R. D. P. Wong, J. D. Posner and V. J. Santos, *Sensors and actuators a: Physical*, 2012, **179**, 62-69.
45. S. Cheng and Z. Wu, *Adv. Funct. Mater.*, 2011, **21**, 2282-2290.
46. R. K. Kramer, C. Majidi, R. Sahai and R. J. Wood, *IEEE/RSJ International Conference on Intelligent Robots and Systems*, San Francisco, September, 2011.
47. E. L. White, J. C. Case and R. K. Kramer, *IEEE Sens. J.*, 2015, **16**, 2607-2616.
48. Q. Gao, H. Li, J. Zhang, Z. Xie, J. Zhang and L. Wang, *Sci. Rep.*, 2019, **9**, 5908.
49. R. K. Kramer, C. Majidi and R. J. Wood, *International Conference on Robots and Automation*, Shanghai, May, 2011.
50. M. Jiang, S. Chen, P. Zhang, Y. Sun, J. Ye, Y. Deng, L. Li and J. Liu, *Mater. Today*, 2023, **66**, 50-61.
51. C. Okutani, T. Yokota, H. Miyazako and T. Someya, *Adv. Mater. Technol.*, 2022, **7**, 2101657.
52. H.-J. Kim, C. Son and B. Ziaie, *Appl. Phys. Lett.*, 2008, **92**, 011904.
53. A. Fassler and C. Majidi, *Smart Mater. Struct.*, 2013, **22**, 055023.
54. N. Pekas, Q. Zhang and D. Juncker, *J. Micromech. Microeng.*, 2012, **22**, 097001.
55. M. Gao and L. Gui, *Lab Chip*, 2014, **14**, 1866-1872.
56. J. Wang, S. Liu and A. Nahata, *Opt. Express*, 2012, **20**, 12119-12126.
57. G. Li, M. Zhang, S. Liu, M. Yuan, J. Wu, M. Yu, L. Teng, Z. Xu, J. Guo, G. Li, Z. Liu and X. Ma, *Nat. Electron.*, 2023, **6**, 154-163.
58. J. Park, S. Wang, M. Li, C. Ahn, J. K. Hyun, D. S. Kim, D. K. Kim, J. A. Rogers, Y. Huang and S. Jeon, *Nat. Commun.*, 2012, **3**, 916.
59. K. P. Mineart, Y. Lin, S. C. Desai, A. S. Krishnan, R. J. Spontak and M. D. Dickey, *Soft Matter*, 2013, **9**, 7695-7700.
60. C. J. Stevens, I. Spanos, A. Vallecchi, J. McGhee and W. Whittow, *Small*, 2022, **18**, 2105368.

61. K. Kim, J. Ahn, Y. Jeong, J. Choi, O. Gul and I. Park, *Micro Nano Syst. Lett.*, 2021, **9**, 1-8.
62. Q. Wu, F. Zhu, Z. Wu, Y. Xie, J. Qian, J. Yin and H. Yang, *npj Flexible Electron.*, 2022, **6**, 50.
63. B. L. Cumby, G. J. Hayes, M. D. Dickey, R. S. Justice, C. E. Tabor and J. C. Heikenfeld, *Appl. Phys. Lett.*, 2012, **101**, 174102.
64. T. Liu, P. Sen and C.-J. Kim, *J. Microelectromech. Syst.*, 2011, **21**, 443-450.
65. T. V. Neumann and M. D. Dickey, *Adv. Mater. Technol.*, 2020, **5**, 2000070.
66. J. W. Boley, E. L. White, G. T. C. Chiu and R. K. Kramer, *Adv. Funct. Mater.*, 2014, **24**, 3501-3507.
67. A. Cook, D. P. Parekh, C. Ladd, G. Kotwal, L. Panich, M. Durstock, M. D. Dickey and C. E. Tabor, *Adv. Eng. Mater.*, 2019, **21**, 1900400.
68. Y.-G. Park, H. S. An, J.-Y. Kim and J.-U. Park, *Sci. Adv.*, 2019, **5**, eaaw2844.
69. C. Ladd, J.-H. So, J. Muth and M. D. Dickey, *Adv. Mater.*, 2013, **25**, 5081-5085.
70. C. Jia and X. Guo, *Chem. Soc. Rev.*, 2013, **42**, 5642-5660.
71. E. Gorenskaia, K. L. Turner, S. Martín, P. Cea and P. J. Low, *Nanoscale*, 2021, **13**, 9055-9074.
72. F. C. Simeone, H. J. Yoon, M. M. Thuo, J. R. Barber, B. Smith and G. M. Whitesides, *J. Am. Chem. Soc.*, 2013, **135**, 18131-18144.
73. R. Haag, M. A. Rampi, R. E. Holmlin and G. M. Whitesides, *J. Am. Chem. Soc.*, 1999, **121**, 7895-7906.
74. K. Slowinski, H. K. Fong and M. Majda, *J. Am. Chem. Soc.*, 1999, **121**, 7257-7261.
75. R. L. York, P. T. Nguyen and K. Slowinski, *J. Am. Chem. Soc.*, 2003, **125**, 5948-5953.
76. Y. Selzer, A. Salomon and D. Cahen, *J. Am. Chem. Soc.*, 2002, **124**, 2886-2887.
77. S. Park and H. J. Yoon, *Nano Lett.*, 2018, **18**, 7715-7718.
78. C. A. Nijhuis, W. F. Reus and G. M. Whitesides, *J. Am. Chem. Soc.*, 2009, **131**, 17814-17827.
79. P. Rothmund, C. Morris Bowers, Z. Suo and G. M. Whitesides, *Chem. Mater.*, 2018, **30**, 129-137.
80. H. J. Um, G. D. Kong and H. J. Yoon, *ACS Appl. Mater. Interfaces*, 2018, **10**, 34758-34764.
81. Z. Zhao, S. Soni, T. Lee, C. A. Nijhuis and D. Xiang, *Adv. Mater.*, 2023, **35**, 2203391.
82. L. Jiang and C. A. Nijhuis, *RSC Adv.*, 2017, **7**, 14544-14551.
83. C. A. Nijhuis, W. F. Reus, J. R. Barber and G. M. Whitesides, *J. Phys. Chem. C*, 2012, **116**, 14139-14150.
84. H. J. Yoon, C. M. Bowers, M. Baghbanzadeh and G. M. Whitesides, *J. Am. Chem. Soc.*, 2014, **136**, 16-19.
85. C. M. Bowers, K.-C. Liao, T. Zaba, D. Rappoport, M. Baghbanzadeh, B. Breiten, A. Krzykawska, P. Cyganik and G. M. Whitesides, *ACS nano*, 2015, **9**, 1471-1477.
86. J. Jang, P. He and H. J. Yoon, *Acc. Chem. Res.*, 2023, **56**, 7715-7718.
87. M. A. Creighton, M. C. Yuen, M. A. Susner, Z. Farrell, B. Maruyama and C. E. Tabor, *Langmuir*, 2020, **36**, 12933-12941.
88. F. Krisnadi, S. Kim, S. Im, D. Chacko, M. H. Vong, K. Rykaczewski, S. Park and M. D. Dickey, *Adv. Mater.*, 2024, 2308862.
89. A. R. Jacob, D. P. Parekh, M. D. Dickey and L. C. Hsiao, *Langmuir*, 2019, **35**, 11774-11783.
90. Y. Lu, Y. Lin, Z. Chen, Q. Hu, Y. Liu, S. Yu, W. Gao, M. D. Dickey and Z. Gu, *Nano Lett.*, 2017, **17**, 2138-2145.
91. A. Elbourne, S. Cheeseman, P. Atkin, N. P. Truong, N. Syed, A. Zavabeti, M. Mohiuddin, D. Esrafilzadeh, D. Cozzolino, C. F. McConville, M. D. Dickey, R. J. Crawford, K. Kalantar-Zadeh, J. Chapman, T. Daeneke and V. K. Truong, *ACS nano*, 2020, **14**, 802-817.
92. M. Pourbaix, *NACE*, 1966.
93. Y. Chung and C.-W. Lee, *J. Electrochem. Sci. Technol.*, 2013, **4**, 1-18.
94. R. A. Bilodeau, D. Y. Zemlyanov and R. K. Kramer, *Adv. Mater. Interfaces*, 2017, **4**, 1600913.
95. M. D. Dickey, *ACS Appl. Mater. Interfaces*, 2014, **6**, 18369-18379.
96. R. Ma, Y. Zhou and J. Liu, *arXiv preprint arXiv:1706.01457*, 2017.
97. G. Li, M. Parmar, D. Kim, J.-B. J. Lee and D.-W. Lee, *Lab Chip*, 2014, **14**, 200-209.
98. G. Li, X. Wu and D.-W. Lee, *Lab Chip*, 2016, **16**, 1366-1373.
99. D. Kim, P. Thissen, G. Viner, D.-W. Lee, W. Choi, Y. J. Chabal and J.-B. Lee, *ACS Appl. Mater. Interfaces*, 2013, **5**, 179-185.
100. B. J. Carey, J. Z. Ou, R. M. Clark, K. J. Berean, A. Zavabeti, A. S. R. Chesman, S. P. Russo, D. W. M. Lau, Z.-Q. Xu, Q. Bao, O. Kavehei, B. C. Gibson, M. D. Dickey, R. B. Kaner, T. Daeneke and K. Kalantar-Zadeh, *Nat. Commun.*, 2017, **8**, 14482.
101. N. Ilyas, D. P. Butcher, M. F. Durstock and C. E. Tabor, *Adv. Mater. Interfaces*, 2016, **3**, 1500665.
102. D. C. Grahame, *Chem. Rev.*, 1947, **41**, 441-501.
103. F. Mugele and J.-C. Baret, *J. Phys.: Condens. Matter*, 2005, **17**, R705.
104. L. Sheng, J. Zhang and J. Liu, *Adv. Mater.*, 2014, **26**, 6036-6042.
105. K. D. Hillaire, P. Nithyanandam, M. Song, S. R. Nadimi, A. Kiani, M. D. Dickey and K. E. Daniels, *Adv. Funct. Mater.*, 2023, 2311501.
106. C. B. Eaker and M. D. Dickey, *Appl. Phys. Rev.*, 2016, **3**, 031103.
107. M. Song, K. E. Daniels, A. Kiani, S. Rashid-Nadimi and M. D. Dickey, *Adv. Intell. Syst.*, 2021, **3**, 2100024.
108. Y. He, J. You, M. D. Dickey and X. Wang, *Adv. Funct. Mater.*, 2023, 2309614.
109. C. B. Eaker, D. C. Hight, J. D. O'Regan, M. D. Dickey and K. E. Daniels, *Phys. Rev. Lett.*, 2017, **119**, 174502.
110. F. F. Yun, Z. Yu, Y. He, L. Jiang, Z. Wang, H. Gu and X. Wang, *Natl. Sci. Rev.*, 2020, **7**, 366-372.
111. Y. He, J. Tang, K. Kalantar-Zadeh, M. D. Dickey and X. Wang, *PNAS*, 2022, **119**, e2117535119.
112. M. Song, K. Kartawira, K. D. Hillaire, C. Li, C. B. Eaker, A. Kiani, K. E. Daniels and M. D. Dickey, *PNAS*, 2020, **117**, 19026-19032.
113. J. H. So, H. J. Koo, M. D. Dickey and O. D. Velev, *Adv. Funct. Mater.*, 2012, **22**, 625-631.
114. H. J. Koo, J. H. So, M. D. Dickey and O. D. Velev, *Adv. Mater.*, 2011, **23**, 3559-3564.
115. J. Norkett, M. Dickey and V. Miller, *Metall. Mater. Trans. A*, 2021, **52**, 2158-2172.
116. S. Liu, D. Qu, S. McDonald, Q. Gu, S. Matsumura and K. Nogita, *J. Alloys Compd.*, 2020, **826**, 154221.
117. S. Liu, K. Sweatman, S. McDonald and K. Nogita, *Materials*, 2018, **11**, 1384.

118. W. Ludsig, D. Bellet, *Mater. Sci. Eng.*, 2000, A281, 198-203.
119. W. Tsai, Y. Hwu, C. Chen, L. Chang, J. Je, H. Lin and G. Margaritondo, *Nucl. Instrum. Methods Phys. Res., Sect. B*, 2003, **199**, 457-463.
120. Y. Cui, F. Liang, Z. Yang, S. Xu, X. Zhao, Y. Ding, Z. Lin and J. Liu, *ACS Appl. Mater. Interfaces*, 2018, **10**, 9203-9210.
121. J. Tang, X. Zhao, J. Li, Y. Zhou and J. Liu, *Adv. Sci.*, 2017, **4**, 1700024.
122. K. B. Ozutemiz, J. Wissman, O. B. Ozdoganlar and C. Majidi, *Adv. Mater. Interfaces*, 2018, **5**, 1701596.
123. G. Li, X. Wu and D.-W. Lee, *Sens. Actuators, B*, 2015, **221**, 1114-1119.
124. G. Li and D.-W. Lee, *Lab Chip*, 2017, **17**, 3415-3421.
125. M. Reis Carneiro, C. Majidi and M. Tavakoli, *Adv. Funct. Mater.*, 2023, **33**, 2306453.
126. Y. Peng, Y. Xin, J. Zhang, M. D. Dickey and Q. Li, *Responsive Materials*, 2023, **1**, e20230003.
127. J. Tang, X. Zhao, J. Li, R. Guo, Y. Zhou and J. Liu, *ACS Appl. Mater. Interfaces*, 2017, **9**, 35977-35987.
128. R. Guo, B. Cui, X. Zhao, M. Duan, X. Sun, R. Zhao, L. Sheng, J. Liu and J. Lu, *Mater. Horiz.*, 2020, **7**, 1845-1853.
129. J. Shu, Y. Lu, E. Wang, X. Li, S.-Y. Tang, S. Zhao, X. Zhou, L. Sun, W. Li and S. Zhang, *ACS Appl. Mater. Interfaces*, 2020, **12**, 11163-11170.
130. D. P. Parekh, C. M. Fancher, M. G. Mohammed, T. V. Neumann, D. Saini, J. Guerrier, C. Ladd, E. Hubbard, J. L. Jones and M. D. Dickey, *ACS Appl. Nano Mater.*, 2020, **3**, 12064-12070.
131. R. Xing, J. Yang, D. Zhang, W. Gong, T. V. Neumann, M. Wang, R. Huang, J. Kong, W. Qi and M. D. Dickey, *Matter*, 2023, **6**, 2248-2262.
132. R. Guo, X. Sun, S. Yao, M. Duan, H. Wang, J. Liu and Z. Deng, *Adv. Mater. Technol.*, 2019, **4**, 1900183.
133. U. Daalkhajav, O. D. Yirmibesoglu, S. Walker and Y. Mengüç, *Adv. Mater. Technol.*, 2018, **3**, 1700351.
134. R. Guo, X. Wang, H. Chang, W. Yu, S. Liang, W. Rao and J. Liu, *Adv. Eng. Mater.*, 2018, **20**, 1800054.
135. C. Wang, Y. Gong, B. V. Cunning, S. Lee, Q. Le, S. R. Joshi, O. Buyukcakir, H. Zhang, W. K. Seong, M. Huang, M. Wang, J. Lee, G.-H. Kim and R. S. Ruoff, *Sci. Adv.*, 2021, **7**, eabe3767.
136. W. Kong, Z. Wang, M. Wang, K. C. Manning, A. Uppal, M. D. Green, R. Y. Wang and K. Rykaczewski, *Adv. Mater.*, 2019, **31**, 1904309.
137. L. Cao, D. Yu, Z. Xia, H. Wan, C. Liu, T. Yin and Z. He, *Adv. Mater.*, 2020, **32**, 2000827.
138. H. Wang, B. Yuan, S. Liang, R. Guo, W. Rao, X. Wang, H. Chang, Y. Ding, J. Liu and L. Wang, *Mater. Horiz.*, 2018, **5**, 222-229.
139. R. Guo, X. Sun, B. Yuan, H. Wang and J. Liu, *Adv. Sci.*, 2019, **6**, 1901478.
140. S. Kim, S. Kim, K. Hong, M. D. Dickey and S. Park, *ACS Appl. Mater. Interfaces*, 2022, **14**, 37110-37119.
141. K. Hong, M. Choe, S. Kim, H.-M. Lee, B.-J. Kim and S. Park, *Polymers*, 2021, **13**, 2407.
142. R. Zhao, H. Dai and H. Yao, *IEEE Rob. Autom. Lett.*, 2022, **7**, 4535-4541.
143. I. D. Joshipura, K. A. Persson, V. K. Truong, J.-H. Oh, M. Kong, M. H. Vong, C. Ni, M. Alsafatwi, D. P. Parekh, H. Zhao and M. D. Dickey, *Langmuir*, 2021, **37**, 10914-10923.
144. I. D. Joshipura, H. R. Ayers, G. A. Castillo, C. Ladd, C. E. Tabor, J. J. Adams and M. D. Dickey, *ACS Appl. Mater. Interfaces*, 2018, **10**, 44686-44695.
145. J. Ma, V. T. Barambe, K. A. Persson, A. L. Bachmann, I. D. Joshipura, J. Kim, K. H. Oh, J. F. Patrick, J. J. Adams and M. D. Dickey, *ACS Appl. Mater. Interfaces*, 2020, **13**, 12709-12718.
146. S. Babu, B. Dousti, G. S. Lee and J.-B. Lee, *Langmuir*, 2021, **37**, 8139-8147.
147. G. Chen, H. Wang, R. Guo, M. Duan, Y. Zhang and J. Liu, *ACS Appl. Mater. Interfaces*, 2020, **12**, 6112-6118.
148. R. Guo, J. Tang, S. Dong, J. Lin, H. Wang, J. Liu and W. Rao, *Adv. Mater. Technol.*, 2018, **3**, 1800265.
149. H. Wang, Y. Zhang, X. He, F. Zuo, Y. Yang, P. Yan, B. Luo and S. He, *Appl. Surf. Sci.*, 2023, **609**, 155410.
150. L. Teng, S. Ye, S. Handschuh-Wang, X. Zhou, T. Gan and X. Zhou, *Adv. Funct. Mater.*, 2019, **29**, 1808739.
151. M. Liao, H. Liao, J. Ye, P. Wan and L. Zhang, *ACS Appl. Mater. Interfaces*, 2019, **11**, 47358-47364.
152. J. E. Park, H. S. Kang, M. Koo and C. Park, *Adv. Mater.*, 2020, **32**, 2002178.
153. B. Qin and U. Schneider, *J. Am. Chem. Soc.*, 2016, **138**, 13119-13122.
154. K. Kalantar-Zadeh, J. Tang, T. Daeneke, A. P. O'Mullane, L. A. Stewart, J. Liu, C. Majidi, R. S. Ruoff, P. S. Weiss and M. D. Dickey, *ACS Nano*, 2019, **13**, 7388-7395.
155. D. C. Upham, V. Agarwal, A. Khechfe, Z. R. Snodgrass, M. J. Gordon, H. Metiu and E. W. McFarland, *Science*, 2017, **358**, 917-921.
156. M. Mayyas, H. Li, P. Kumar, M. B. Ghasemian, J. Yang, Y. Wang, D. J. Lawes, J. Han, M. G. Saborio, J. Tang, R. Jalili, S. H. Lee, W. K. Seong, S. P. Russo, D. Esrafilzadeh, T. Daeneke, R. B. Kaner, R. S. Ruoff and K. Kalantar-Zadeh, *Adv. Mater.*, 2020, **32**, 2001997.
157. D. Esrafilzadeh, A. Zavabeti, R. Jalili, P. Atkin, J. Choi, B. J. Carey, R. Brkljača, A. P. O'Mullane, M. D. Dickey, D. L. Officer, D. R. MacFarlane, T. Daeneke and K. Kalantar-Zadeh, *Nat. Commun.*, 2019, **10**, 865.
158. J. Tang, A. J. Christofferson, J. Sun, Q. Zhai, P. V. Kumar, J. A. Yuwono, M. Tajik, N. Meftahi, J. Tang, L. Dai, G. Mao, S. P. Russo, R. B. Kaner, M. A. Rahim and K. Kalantar-Zadeh, *Nat. Nanotechnol.*, 2024, **19**, 306-310.
159. M.-g. Kim, B. Lee, M. Li, S. Noda, C. Kim, J. Kim, W.-J. Song, S. W. Lee and O. Brand, *ACS nano*, 2020, **14**, 5659-5667.
160. L. Hu, L. Wang, Y. Ding, S. Zhan and J. Liu, *Adv. Mater.*, 2016, **28**, 9210-9217.
161. C. Wang, Y. Gong, B. V. Cunning, S. Lee, Q. Le, S. R. Joshi, O. Buyukcakir, H. Zhang, W. K. Seong and M. Huang, *Science advances*, 2021, **7**, eabe3767.
162. L. Peng, Y. Su, X. Yang and G. Sui, *J. Colloid Interface Sci.*, 2023, **638**, 313-323.
163. Y. Xin, Y. Lou, X. Mao, X. Jia, R. Li, P. Yu and X. Ban, *Macromol. Rapid Commun.*, 2023, **44**, 2300307.
164. E. J. Frey, S. Im, A. L. Bachmann, J. Genzer and M. D. Dickey, *Adv. Funct. Mater.*, 2023, 2308574.
165. D. Wang, X. Wang and W. Rao, *Acc. Mater. Res.*, 2021, **2**, 1093-1103.

ARTICLE

Journal Name

166. Y.-G. Park, H. Min, H. Kim, A. Zhexembekova, C. Y. Lee and J.-U. Park, *Nano Lett.*, 2019, **19**, 4866-4872.
167. W. Xing, S. Chen, H. Wang, W. Liu, J. Zheng, F. Zheng, X. Li, P. Tao, W. Shang, B. Fu, C. Song, B. Li and T. Deng, *Adv. Mater. Technol.*, 2022, **7**, 2100970.
168. R. K. Kramer, J. W. Boley, H. A. Stone, J. C. Weaver and R. J. Wood, *Langmuir*, 2014, **30**, 533-539.
169. D. Kim, D.-W. Lee, W. Choi and J.-B. Lee, *J. Microelectromech. Syst.*, 2013, **22**, 1267-1275.
170. Y. Jiang, S. Su, H. Peng, H. S. Kwok, X. Zhou and S. Chen, *J. Mater. Chem. C*, 2017, **5**, 12378-12383.
171. S. Zhang, B. Wang, J. Jiang, K. Wu, C. F. Guo and Z. Wu, *ACS Appl. Mater. Interfaces*, 2019, **11**, 7148-7156.
172. J. Zhang, K. Zhang, J. Yong, Q. Yang, Y. He, C. Zhang, X. Hou and F. Chen, *J. Colloid Interface Sci.*, 2020, **578**, 146-154.
173. G. Li, M. Parmar and D.-W. Lee, *Lab Chip*, 2015, **15**, 766-775.
174. A. Hirsch and S. P. Lacour, *Adv. Sci.*, 2018, **5**, 1800256.
175. J.-H. Kim, S. Kim, H. Kim, S. Wooh, J. Cho, M. D. Dickey, J.-H. So and H.-J. Koo, *Nat. Commun.*, 2022, **13**, 4763.